

# Galaxies in a simulated $\Lambda$ CDM Universe I: cold mode and hot cores

Dušan Kereš<sup>1,2</sup>, Neal Katz<sup>2</sup>, Mark Fardal<sup>2</sup>, Romeel Davé<sup>3</sup>, David H. Weinberg<sup>4</sup>

<sup>1</sup>*Institute for Theory and Computation, Harvard-Smithsonian Center for Astrophysics, Cambridge, MA 02138, dkereš@cfa.harvard.edu*

<sup>2</sup>*Astronomy Department, University of Massachusetts at Amherst, MA 01003; nsk@kaka.astro.umass.edu, fardal@astro.umass.edu*

<sup>3</sup>*University of Arizona, Steward Observatory, Tucson, AZ 85721; rad@astro.as.arizona.edu*

<sup>4</sup>*Ohio State University, Department of Astronomy, Columbus, OH 43210; dhw@astronomy.ohio-state.edu*

1 November 2021

## ABSTRACT

We study the formation of galaxies in a large volume ( $50h^{-1}$  Mpc,  $2 \times 288^3$  particles) cosmological simulation, evolved using the entropy and energy conserving smoothed particle hydrodynamics (SPH) code GADGET-2. Most of the baryonic mass in galaxies of all masses is originally acquired through filamentary “cold mode” accretion of gas that was never shock heated to its halo virial temperature, confirming the key feature of our earlier results obtained with a different SPH code (Kereš et al. 2005). Atmospheres of hot, virialized gas develop in halos above  $2 - 3 \times 10^{11} M_{\odot}$ , a transition mass that is nearly constant from  $z = 3$  to  $z = 0$ . Cold accretion persists in halos above the transition mass, especially at  $z \geq 2$ . It dominates the growth of galaxies in low mass halos at all times, and it is the main driver of the cosmic star formation history. Our results suggest that the cooling of shock-heated, virialized gas, which has been the focus of many analytic models of galaxy growth spanning more than three decades, might be a relatively minor element of galaxy formation. At high redshifts, satellite galaxies have gas accretion rates similar to central galaxies of the same baryonic mass, but at  $z < 1$  the accretion rates of low mass satellites are well below those of comparable central galaxies. Relative to our earlier simulations, the GADGET-2 simulations predict much lower rates of “hot mode” accretion from the virialized gas component. Hot accretion rates compete with cold accretion rates near the transition mass, but only at  $z \leq 1$ . Hot accretion is inefficient in halos above  $\sim 5 \times 10^{12} M_{\odot}$ , with typical rates lower than  $1 M_{\odot} \text{ yr}^{-1}$  at  $z \leq 1$ , even though our simulation does not include AGN heating or other forms of “preventive” feedback. Instead, the accretion rates are low because the inner density profiles of hot gas in these halos are shallow, with long associated cooling times. The cooling recipes typically used in semi-analytic models can overestimate the accretion rates in these halos by orders of magnitude, so these models may overemphasize the role of preventive feedback in producing observed galaxy masses and colors. A fraction of the massive halos develop cuspy profiles and significant cooling rates between  $z = 1$  and  $z = 0$ , a redshift trend similar to the observed trend in the frequency of cooling flow clusters.

**Key words:** cooling flows — feedback — cluster – galaxies: evolution — galaxies: formation — models: semi-analytic — models: numerical

## 1 INTRODUCTION

The wealth of high quality observational galaxy data at different epochs, from the earliest times to the present, has rapidly grown in the last several years. This provides a great opportunity to calibrate and improve our theoretical understanding of galaxy formation and evolution. One of the re-

maining challenges in theoretical extragalactic astronomy is the origin of the bimodality in galactic properties: massive galaxies that are typically red, elliptical systems with very little star formation, and lower mass galaxies that are typically blue, disk, star forming systems (e.g. Kauffmann et al. 2003; Baldry et al. 2004). Usually one invokes various feed-

back processes to shut down star formation in massive galaxies, which enables them to populate the red sequence (see review in Hopkins et al. 2008). In addition, without feedback in the low mass galaxies, a large fraction of baryons would cool and form stars, even at very early times (White & Rees 1978), contrary to the small fraction of baryons in observed galaxies (e.g. Bell et al. 2003).

To understand where, when, and to what degree we need feedback during galaxy formation and evolution, we first have to understand how galaxies are supplied with baryons, and in particular with the gas that provides the fuel for star formation. In our previous work (Kereš et al. 2005, K05 hereafter), we showed that it is the smooth accretion of intergalactic gas that dominates the global galactic gas supply, not accretion by merging, and that it proceeds via two stages. First, gas is accreted through filamentary streams, where it remains relatively cold before it reaches the galaxy (Katz et al. 2003, K05). This process, which we call cold mode accretion, is very efficient, and because the gas does not need to cool it falls in on approximately a free-fall time. This means that the baryonic growth closely tracks the growth of the dark matter halo, albeit with a slight time delay. Cold mode accretion dominates the global growth of galaxies at high redshifts and the growth of lower mass objects at late times. As the dark matter halo grows larger, a larger fraction of the infalling material shock heats to temperatures close to the virial temperature. In the denser, central regions a fraction of this hot gas is able to cool. This process, virial shock heating followed by radiative cooling, is the one highlighted in classic papers on galaxy formation theory (e.g. Rees & Ostriker 1977; Silk 1977; White & Rees 1978; White & Frenk 1991), and to differentiate it from the previous mode we call it hot mode accretion. In massive halos, this hot mode accretion not only supplies massive galaxies with fresh gas but could also be identified as cluster cooling flows (e.g. Fabian 1994), although observations suggest that cooling in most clusters does not actually reach down to galactic temperatures, perhaps because of heating by AGN or some other feedback mechanism (e.g. McNamara & Nulsen 2007). The dominant accretion mode depends on halo mass, and the transition between these two regimes occurs at a mass of about  $M_{\text{halo}} = 2 - 3 \times 10^{11} M_{\odot}$ . At higher redshifts, cold filaments are able to survive within halos above this transition mass, i.e. halos dominated by hot halo gas. Overall, the bulk of the baryonic mass in galaxies is accreted through the cold accretion mode.

Cold accretion owes its existence to the short cooling times present in low mass halos near the virial radius, which prevents the development of a stable accretion shock. The detailed criteria required to prevent the formation of a virial shock in low mass idealized systems have been derived by Binney (1977) and Birnboim & Dekel (2003). However, in cosmological simulations the situation is more complex than in these simple models. For example, the spherical symmetry assumed in the case of Birnboim & Dekel (2003) will not be valid owing to the presence of dense, cold filaments that dramatically enhance the density contrasts in the gas and shorten the cooling times. In halos with masses near the transition mass from cold to hot mode, this allows cold filamentary flows to still supply the central galaxy with gas even though some of the infalling gas shock heats to near the virial temperature.

There are two main classes of galaxy formation feedback processes: those that prevent gas from entering a galaxy in the first place, “preventive” feedback, and those that expel a fraction of the gas that does manage to enter the galaxy, “ejective” feedback. AGN “radio mode” heating is an example of preventive feedback (e.g. Best et al. 2005; Croton et al. 2006) and winds driven by supernovae are an example of ejective feedback (e.g. Dekel & Silk 1986; Springel & Hernquist 2003). The effectiveness of these two feedback types will vary depending on the dominant accretion mode in the halo hosting the galaxy. Because cold mode halos have very little halo gas outside of the cold dense filaments, it is not clear if feedback processes can drastically affect the accretion of gas. Ejective feedback, such as galactic winds driven by supernovae, could still lower the masses of galaxies by expelling already accreted material. Such winds, however, might be stopped by the quasi-spherical, hot halos that surround hot mode galaxies. Conversely, preventive feedback, like the AGN radio mode, is likely only effective in hot mode halos, where it can prevent the hot, dilute gas that is in quasi-static equilibrium from cooling. Similar constraints apply for the “quasar wind mode” of AGN feedback (Di Matteo et al. 2005), which could possibly be a mixture of these two feedback modes. At first, a relatively small fraction of galaxy mass is ejected in the quasar wind, but later the energy released from the black hole accretion could in principle provide “preventive” feedback if the quasar was active within a halo that has a hot quasi-spherical atmosphere. In summary: ejective feedback is likely to be most effective in cold mode halos, and preventive feedback is likely to be effective only in hot mode halos. An exception to this rule is “pre-heating” of intergalactic gas by photoionization (Efstathiou 1992; Quinn et al. 1996; Thoul & Weinberg 1996), or gravitational shocks (Mo et al. 2005), which is a form of preventive feedback that will mostly affect low mass, cold mode halos.

Current cosmological simulations have insufficient resolution (often by large margins) to predict these feedback processes from first principles, though they may incorporate simplified recipes designed to achieve these effects. It is, therefore, important to gain a general understanding of when and where these two classes of feedback processes are needed to explain the observed properties of galaxies. In this paper, we examine the growth of galaxies by gas accretion and the dependence of this process on galaxy mass, halo mass, and redshift. In a companion paper (Keres et al. 2009, Paper II, hereafter), we compare the observable properties of our simulated galaxies, such as stellar masses and specific star formation rates, to current data.

In K05 we showed that the mass of the transition from cold to hot mode accretion does not depend much on the resolution of the cosmological simulation. However, we showed that increasing the mass and spatial resolution substantially reduced the amount of hot mode accretion. This suggested that the simulations from K05 had too much hot mode accretion, perhaps the result of numerical problems inherent in the Smoothed Particle Hydrodynamics (SPH) formulation that we used (see Springel & Hernquist 2002, SH02 hereafter, for a brief review). How much gas is able to cool from the hot atmosphere remained, therefore, an unanswered question in K05. In this paper, we use the GADGET-2SPH code (Springel 2005) because it does not suffer from

numerical overcooling in massive halos, as we demonstrate in Kereš et al. (2009b, in preparation) and in Keres (2007), and because it parallelizes more efficiently to large numbers of processors. The SPH algorithm implemented in GADGET-2, which simultaneously conserves entropy and energy, is a reliable method for simulations of cosmologically relevant volumes where galaxies are often only resolved with a small number of particles. In our previous simulations, this low resolution allowed a mixing of the cold and hot gas phases, which led to an artificial increase in the cooling rates and an overestimate of the hot mode accretion (Pearce et al. 2001; Croft et al. 2001). In our new GADGET-2simulations, we show that a large fraction of the massive, hot mode halos cannot cool their gas, owing to nearly uniform density cores that develop in these halos. However, as discussed below (§3.4), GADGET-2simulations may still suffer numerical problems that distort gas accretion rates, albeit at lower magnitude; fully understanding these effects will require tests beyond those in this paper. Relative to K05, we also increase the simulation volume by about an order of magnitude, allowing much better statistics for high mass halos and galaxies. We use a similar but slightly better mass resolution.

Here we present theoretical predictions of galaxy masses and accretion rates in cosmological simulations without strong feedback. The energy from supernovae pressurizes the interstellar medium, but it does not drive large scale outflows. We do not include any other feedback mechanisms that could prevent the accretion of gas or that could expel gas from galaxies in the mass range of interest in this paper. The only exception is that we include an extragalactic UV background, which affects the intergalactic medium and reduces gas accretion in the lowest mass halos.

In the Paper II we confirm earlier findings that the amount of material that cools onto galactic component is too high in simulations such as ours, which causes galaxies at any mass, but especially at the low and high mass end to be more massive than their observed counterparts. There we argue that an efficient high redshift feedback in low mass galaxies (perhaps with the addition of low redshift AGN feedback) is the key for getting the correct galaxy masses.

Many of the results in this paper and its companions (Paper II, and Keres et al. 2009b (in preparation)) first appeared as part of D. Kereš's PhD thesis at University of Massachusetts, Amherst (Keres 2007).

In §2 we describe the basic parameters and setup of our new simulations. In §3 we describe the smooth accretion of gas, both globally and for individual objects. In §4 we describe the properties of non-cooling and cooling halos and conclude in §5.

## 2 SIMULATIONS

We adopt a cold dark matter model dominated by a cosmological constant,  $\Lambda$ CDM. In K05 we studied the properties of gas accretion in galaxies and their growth using an older version of the  $\Lambda$ CDM cosmology. Data from the first 3 years of the WMAP mission (Spergel et al. 2007) suggest much lower values of  $\sigma_8$  and  $\Omega_m$  (as anticipated by the galaxy clustering analyses of van den Bosch et al. (2003) and Tinker et al. (2005)), which slightly changes the time and redshift depen-

dence of structure and galaxy growth. We therefore use the following cosmological parameters:  $\Omega_m = 0.26$ ,  $\Omega_\Lambda = 0.74$ ,  $h \equiv H_0/(100 \text{ km s}^{-1} \text{ Mpc}^{-1}) = 0.71$ , and a primordial power spectrum index of  $n = 1.0$ . For the amplitude of the mass fluctuations we use  $\sigma_8 = 0.75$ , and for the baryonic density we adopt  $\Omega_b = 0.044$ . All of these cosmological parameters are consistent with recent measurements from the WMAP team (Spergel et al. 2007) and with various large scale structure measurements<sup>1</sup>, except the primordial power spectrum index which is slightly higher in our simulations. We model a  $50.0h^{-1}$  Mpc comoving periodic cube using  $288^3$  dark matter and  $288^3$  gas particles, i.e. around 50 million particles in total. Gravitational forces are softened using a cubic spline kernel of comoving radius  $10h^{-1}$  kpc, approximately equivalent to a Plummer force softening of  $\epsilon_{\text{grav}} = 7.2h^{-1}$  kpc. Using the naming scheme from K05, we will refer to this simulation as L50/288 later throughout the text. We occasionally compare this simulation to a GADGET-2simulation of a smaller volume simulation, L22/128. This simulation uses the same cosmological parameters and initial conditions as those that were used in K05. To test for resolution effects we also use L11/64 and L11/128 simulations, again with the same initial conditions as their analogs in K05 but simulated with GADGET-2. The parameters of all of these simulations are shown in Table 1. For the visualizations of cold accretion in §3.3 below, we use a higher resolution simulation, L12.5/288, which is described there.

The initial conditions are evolved using the SPH code GADGET-2(Springel 2005). The calculation of the gravitational force is a combination of the Particle Mesh algorithm (e.g. Hockney & Eastwood 1981) for large distances and the hierarchical tree algorithm (Barnes & Hut 1986; Hernquist 1987) for small distances. The smoothed particle hydrodynamics algorithm (Lucy 1977; Gingold & Monaghan 1977) used here is entropy and energy conserving, and it is based on the version used in Springel & Hernquist (2002). We use a modified public version of the GADGET-2. Modifications are made to include the cooling, the uniform UV background and the two-phase star formation algorithm. We briefly describe these below.

We include all the relevant cooling processes with primordial abundances as in Katz et al. (1996). We do not include any metal enrichment or cooling processes associated with heavy elements or molecular hydrogen. In all of these simulations we include a spatially uniform, extragalactic UV background that heats and ionizes the gas. The redshift distribution and spectrum of this background is slightly different than in K05. The background flux starts at  $z = 9$  and is based on Haardt & Madau (2001). For more details about the calculation of this UV background see Oppenheimer & Davé (2006). We note, however, that smaller volume simulations of comparable resolution with our new UV background and with the version used in K05 showed no noticeable differences in the evolution of the galaxy population above our resolution limit in the redshift range of interest in this paper,  $z = 0$  to 4.

Once a gas particle reaches a density above the

<sup>1</sup> <http://lambda.gsfc.nasa.gov/product/map/dr2/parameters.cfm> (see the  $\Lambda$ CDM/All values)

Name	$L(h^{-1} \text{ Mpc})$	$N$	$z_{\text{fin}}$	$m_{\text{gas}}(M_{\odot})$
<b>L50/288</b>	50	$2 \times 288^3$	0	$9 \times 10^7$
L22/128	22.22	$2 \times 128^3$	0	$1.1 \times 10^8$
L11/64	11.11	$2 \times 64^3$	1	$1.1 \times 10^8$
L11/128	11.11	$2 \times 128^3$	1	$1.3 \times 10^7$

**Table 1.** Details of the simulations used in this paper.  $L$  is the comoving box size,  $N$  is the total number of particles (dark+baryonic),  $z_{\text{fin}}$  is the final redshift to which the simulation has been evolved and  $M_{\text{gas}}$  is the initial mass of gas particles in these simulations

star forming threshold, star formation proceeds in a sub-resolution two-phase medium where supernova energy released by type II SNe during star formation balances cold cloud formation and cloud evaporation by the hot medium as in McKee & Ostriker (1977). Pressurization of the interstellar medium by SN feedback enables more stable gas rich disks, but it does not produce a large scale outflow, i.e. a galactic wind. We use the same star formation model parameters as in Springel & Hernquist (2003), which were selected to match the  $z = 0$  relation between star formation rate and gas surface density (Kennicutt 1998; see also Schmidt 1959). The code calculates the threshold density for star formation as the density where the mass weighted temperature of the two phase medium equals 10,000K. In practice this threshold density is constant in physical units during the simulation, and it corresponds to a hydrogen number density of  $n_h = 0.13 \text{ cm}^{-3}$ . Each gas particle within the two-phase medium has an assigned star formation rate, but the actual conversion from gaseous to stellar particles proceeds stochastically (Springel & Hernquist 2003). This is similar to the algorithm in Katz (1992), where each star particle takes half of the initial mass of a gas particle.

To identify bound groups of cold, dense baryonic particles and stars we use the program SKID<sup>2</sup> (see K05 for more details). Briefly, a galaxy identified by SKID contains bound stars and gas with an overdensity  $\rho/\bar{\rho}_{\text{baryon}} > 1000$  and temperature  $T < 30,000 \text{ K}$ . Here, we slightly modify this criterion and apply a higher temperature threshold at densities where the two-phase medium develops. Such a modification is necessary to allow star forming two-phase medium particles to be part of a SKID group, since at high densities the mass-weighted temperature in the two phase medium can be much higher than 30,000 K. To identify halos we use both the Friends of Friends (FOF) and Spherical Overdensity (SO) algorithms with the same parameters as in K05, adjusted to the new cosmology.

### 3 ACCRETION RATES

The baryonic masses  $M_{\text{gal}}$  of SKID galaxies include stars, star-forming (two-phase medium) gas, and gas with  $\rho/\bar{\rho}_{\text{baryon}} > 1000$  and temperature  $T < 30,000 \text{ K}$ . Using the convergence tests in Murali et al. (2002) as a guide, we adopt  $M_{\text{gal}} = 64m_{\text{SPH}}$  as our nominal resolution limit, above which galaxy baryonic masses are reasonably well converged. For the L50/288 simulation,  $m_{\text{SPH}} = 9.1 \times 10^7 M_{\odot}$ , making the resolution criterion  $M_{\text{gal}} \geq 5.8 \times 10^9 M_{\odot}$ . To define accretion rates we require a galaxy to be resolved at both ends of the

time interval used to calculate the rate. This leaves us with around 10,000 resolved galaxies at  $z \leq 2$ . To avoid counting the accretion of sub-resolution groups as a smooth accretion, we define smooth gas accretion as the accretion of gas particles that were not part of any SKID identified group at the previous time, i.e. even bound groups smaller than 64 particles will not be counted as smooth gas accretion. In practice this procedure will avoid counting sub-resolution mergers down to galaxies with  $\sim 20 - 30$  particles, i.e.  $\sim 2 \times 10^9 M_{\odot}$ , approximately the value where the galaxy mass function in our L50/288 simulation drops rapidly owing to our limited resolution and the UV background.

As in K05, we follow the temperature history of the accreted particles, noting the maximum temperature a gas particle reaches before it becomes part of a galaxy,  $T_{\text{max}}$ . We ignore the temperature while a particle is in the two-phase medium for gas particles that are “recycled” from one galaxy to another. Following K05, we also split the smooth accretion into two components, that with  $T_{\text{max}} < 250,000 \text{ K}$ , representing cold mode gas accretion, and that with higher  $T_{\text{max}}$ , representing hot mode accretion. K05 found this to be a good empirical division between the cold and hot accretion modes, and they argued that a cut in physical temperature describes the simulations better than a cut in scaled temperature  $T_{\text{max}}/T_{\text{vir}}$ .

#### 3.1 Global accretion rates

We calculate the global smooth gas accretion rates as the sum of gas accreted by all resolved galaxies at a given time divided by the simulation volume. Following K05 we show results for the  $T_{\text{max}}$  distribution of the global accretion in Figure 1. Global accretion is dominated by the cold mode accretion peak, i.e. by gas accreted with  $T_{\text{max}} \leq 250,000 \text{ K}$ , at all redshifts including  $z = 0$ . The temperature minimum that separates cold from hot mode accretion washes out after  $z \sim 2$ , caused by the very weak hot mode accretion in this new simulation, as we discuss below. As mentioned earlier, SPH codes without second-order entropy conservation can greatly overestimate hot mode accretion (SH02). This problem was hinted at in the high resolution simulations evolved with P-TreeSPH in K05. A careful comparison between simulations that use the same cosmological parameters and initial conditions but different SPH formulations shows that the much lower hot mode accretion rates we find in this new simulation are mostly the consequence of the different SPH formulation (Kereš et al. 2009b, in preparation). We see that the global accretion rate declines towards lower redshift, as we also saw in K05. The change in cosmology also changes the magnitude of the global accretion rates, making high redshift accretion less pronounced than

<sup>2</sup> <http://www-hpcc.astro.washington.edu/tools/skid.html>

in K05 because low  $\sigma_8$  causes structure to form later. Later halo formation, slightly higher mass resolution, and a higher baryon-to-dark-matter ratio all contribute to the higher cold mode accretion rates seen at low redshift.

The change in magnitude of the accretion rates with time is better illustrated in Figure 2, where we show the total smooth gas accretion rates, the cold mode accretion rates, and the hot mode accretion rates. The accretion rates peak around  $z = 3$  followed by a drop to  $z = 0$  of about a factor of 10. The high redshift accretion rates at  $z \sim 4 - 5$  are lower by about a factor of 2-3 in L50/288 compared to K05. The much lower accretion rates result from the later formation time of halos at a given mass, which in turn results from the lower value of  $\sigma_8$  in the new WMAP cosmology. At high redshifts, this later halo formation time results in a smaller number of galaxies that are included in the resolved galaxy sample. Since high redshift accretion is completely dominated by efficient cold mode accretion, the magnitude of these rates approximately reflects the growth of the dark matter halos that host the resolved galaxies (minus the small contribution from sub-resolution mergers), as demonstrated in K05.

The fast increase in the number of galaxies that cross the resolution limit causes the sharp rise in global accretion from  $z \sim 7 - 8$  to  $z \sim 3$ . (Note, however, that we only count accretion onto pre-existing galaxies, so the first appearance of a galaxy above the threshold does not contribute to the accretion rate.) As time increases, the typical accretion rate at fixed galaxy mass declines, but at high redshifts this trend is overwhelmed by the larger number of resolved galaxies and by the increase in average galaxy mass (with higher mass galaxies having higher mean accretion rates). At lower redshifts, the number of resolved galaxies does not change significantly, and the decrease in the average accretion rate at fixed galaxy mass causes a drop in the global accretion rate.

In Figure 2 we also compare the rate of mass growth through mergers to that through smooth accretion. Here, we include as mergers all the material that is added to resolved galaxies between two simulation outputs that is not smoothly accreted. Almost all of the material that is counted as mergers joins the galaxies in dense baryonic clumps. Similar to the findings in K05, mergers dominate the total mass growth at low redshift, in this case after around  $z = 1$ . The gaseous part of the merger rates is now significantly higher than in our previous work. This is largely caused by counting the accretion of small, under-resolved, gas rich galaxies as mergers and in part by the later formation of halos and galaxies, which keeps them slightly more gas rich at late times. However, the gas added through mergers is always significantly lower than that added through smooth accretion. In a global sense, therefore, galaxies are supplied with gas, the fuel for star formation, mainly by smooth accretion.

As in K05, the global star formation rate closely follows the smooth gas accretion rate with a relatively short time delay. This is a consequence of the continuous gas supply and the relatively short, observationally motivated star formation time scale we adopt here. On a galaxy by galaxy basis, there are systematic offsets from this tight relation between the star formation rate and the smooth gas accretion rate, which we will discuss later in this section (see §3.7). Interestingly, the  $z = 0$  global SFR is within a factor of two of

the observed value (Hopkins & Beacom 2006) even though we do not include either supernova winds or AGN feedback. At higher redshifts the observational estimates have an extremely wide range, and while our predicted star formation rates lie within this range, the uncertainty of the comparisons prevents strong constraints on the models.

However, the observed star formation history is quite uncertain and, therefore, matching it at some given time is not necessarily a major success of a given model. A more constraining measure of previous baryonic mass accumulation is the amount of baryons that are locked in the galactic component. We plot the mass accumulation history of baryons in resolved galaxies as a fraction of baryonic density of the universe in Figure 2. At  $z = 0$ , in our L50/288 simulation around 20 percent of available baryons reside in galaxies and around 17 percent of all baryons are locked in stellar component (in and out of galaxies). For the resolved galaxies only, these numbers are 19 and 16 percents, respectively. This is factor of 3 higher than what is observed (Bell et al. 2003), which suggests that, globally, too much gas cools onto galaxies in our simulations. This problem is the main topic of Paper II, where we explore this discrepancy more quantitatively and suggest what kind of feedback is needed to reconcile these differences. Here we only note that the amount of cooled baryons in the simulation analyzed here is lower than what was suggested in earlier work based on SPH simulations without ejective feedback (e.g. Benson et al. 2001). A large part of this difference owes to the use of the entropy and energy conserving code that prevents numerical overcooling in our paper, but additional effects likely owe to the lack of metal cooling in our simulation, the inclusion of a UV background which suppresses the formation of the smallest objects, and a lower  $\sigma_8$  which delays the formation times of halos.

### 3.2 Virialization of the halo gas

Before we proceed to discuss the accretion rates of individual galaxies in our simulation, it is interesting to check if the transition mass between halos dominated by cold filamentary flows and hot virialized gas occurs at a mass similar to that in K05, i.e.  $2 - 3 \times 10^{11} M_\odot$ . For this purpose, Figure 3 plots the fraction of halo gas (excluding gas in SKID-identified galaxies) that is below the temperature that we use to divide cold and hot mode accretion, 250,000 K. We see that cold halo gas remains the dominant component in halos with masses lower than  $2 - 3 \times 10^{11} M_\odot$ , while for higher mass halos hot gas begins to dominate, and the most massive halos are almost completely filled with hot gas. The transition mass between cold and hot halos is almost constant with redshift even though the virial temperature of a halo of a given mass increases with redshift roughly as  $T_{\text{vir}}(z) \propto (1+z)$ . One can also see that hot, virialized gas builds up gradually, with the transition occurring over more than an order of magnitude in halo mass. There is a large density contrast between filaments and the inter-filamentary region, which allows cold mode accretion to coexist with hot gas in the regions between the filaments in this transition mass range. The spherical model of Birnboim & Dekel (2003) predicts an approximately similar transition mass, smaller by a factor of 2 - 3 (though this depends on the precise definition of the transition in their model). Even in

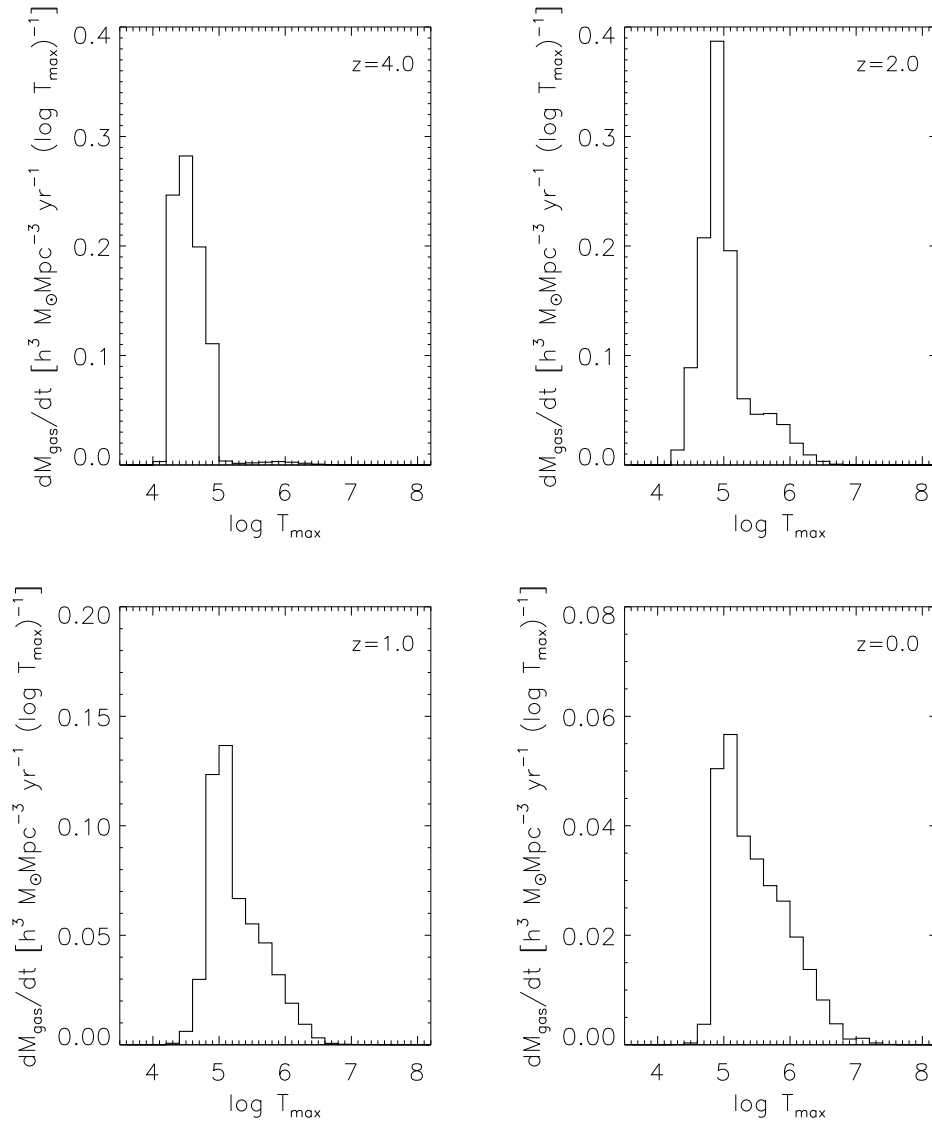


**Figure 1.** The global volume averaged smooth gas accretion rates as a function of  $T_{\max}$  for the L50/288 simulation. The histograms are calculated by adding the mass of all gas particles that were smoothly accreted in a given  $T_{\max}$  bin between two simulation outputs. Note that we express the accretion rates per decade in  $T_{\max}$ , unlike in K05 where they were expressed per bin.

this idealized model, the virial shock expands outwards as the halo mass increases, approximately mimicking the simulations. However, their model does not account for the filamentary structure of the infalling gas, which makes the transition between cold and hot halos sharper than in the cosmological simulations. We also compared the halo cold gas fractions in the simulations used in K05 with the L22/128 and L11/128 simulations, which used the same initial conditions but were evolved with GADGET-2, and we find very similar results.

In summary, as the halo mass increases the hot virialized atmosphere slowly accumulates until it becomes the dominant halo gas component in massive halos. In agreement with K05, we visually confirm (see §3.3) that cold filamentary streams survive in halos with masses much larger than the transition mass, especially at high redshifts, which makes the transition from cold to hot domination a gradual

one and makes the cold gas fraction in massive halos slightly increase with redshift. Ocvirk et al. (2008) and Dekel et al. (2009) show similar results obtained with an adaptive refinement mesh hydrodynamic code. At lower redshifts, the cold-to-hot transition is sharper, but it is also more sensitive to our precise definition because the virial temperature of the halos at the transition mass approaches 250,000 K. Croton et al. (2006) suggest that the transition masses in K05 are biased high owing to the “geometric” SPH method in P-TreeSPH that was used to evolve the simulations. The results from the energy and entropy conserving GADGET-2 simulation that we present here demonstrates clearly that this transition mass is not sensitive to the SPH method used. The transition mass depends, however, on the fraction of halo baryons available in a halo and on the gas metallicity as discussed by Birnboim & Dekel (2003). In our L50/288 simulation, in halos with  $10^{11} M_{\odot} < M_h < 5 \times 10^{11} M_{\odot}$ , typ-

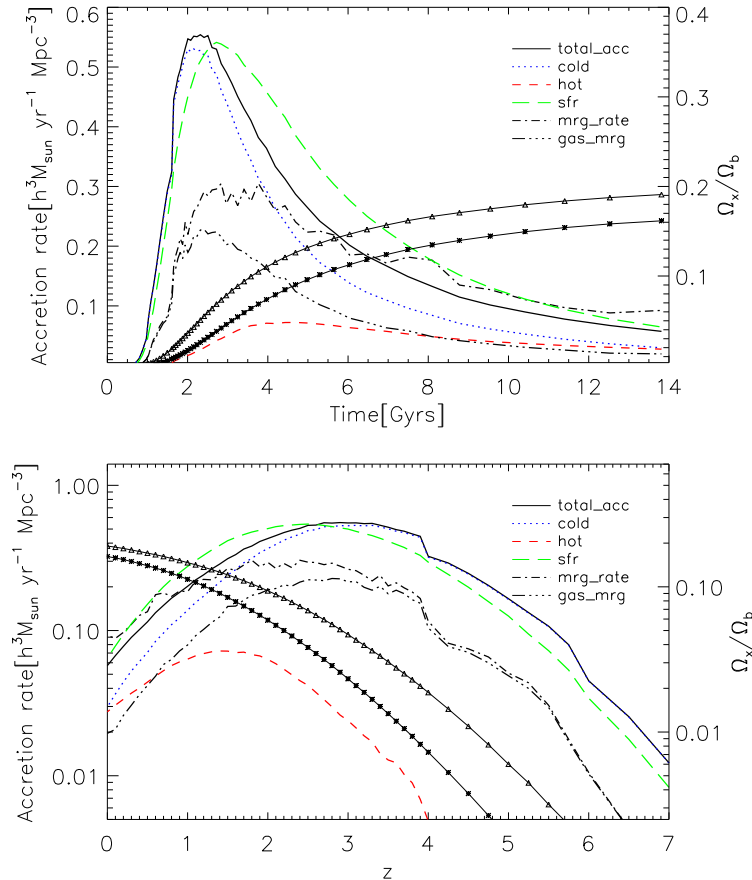


**Figure 2.** The volume averaged smooth gas accretion, star formation and merger rates of the resolved galaxy population in the L50/288 simulation. We show the volume averaged total smooth gas accretion rates (solid), smooth accretion in cold mode (dotted, blue) and smooth accretion in hot mode (dashed, red). We also plot the star formation rate densities of the resolved galaxy population (green, long-dashed), the volume averaged rates of mass increase through mergers (dot-dashed) and the gaseous part of the merger rates (triple-dot-dashed). The upper panel plots the rates versus cosmic time and the lower panel plots the rates versus redshift. In both panels we also overplot the fraction of baryons locked in resolved galaxies (triangles) and the fraction of baryons locked in stars in resolved galaxies (stars), with the corresponding values on the right hand side y-axis.

ically around 40 percent of the halo baryons are residing out of the galactic component. Our preliminary results from simulations that include the metal line cooling and supernova driven galactic winds, which increase the amount of gas in halos, indicate that the transition between halos dominated by cold and hot gas shifts upward by a factor  $\sim 3$  in halo mass.

### 3.3 Illustrations of Cold Mode Accretion

How do filaments that are driving the cold mode accretion connect to galaxies and halos? How do these connections depend on halo mass and redshift? The answers to these questions depend somewhat on numerical resolution. In higher resolution simulations, the central cores of filaments are able to reach higher densities and therefore cool faster and become thinner. Furthermore, the low mass galaxies and subhalos that can be tracked at higher resolution can drag or disturb cold gas filaments in their parent halos. To investi-

gate the qualitative behavior of filamentary cold accretion, we therefore use the highest resolution simulation currently available to us, evolved to  $z = 1$  with  $288^3$  particles in a  $12.5h^{-1}$  Mpc comoving box (L12.5/288). This simulation has no ejective feedback, but it was evolved with metal line cooling and stellar mass loss that gets recycled into the surrounding gas. The detailed properties of the galaxies that form in this simulation will be presented in future work, but it is worth mentioning that this extra physics does not make a significant difference to the properties of the intergalactic halo gas, since without winds the metals and recycled material stay within or close to galaxies. We explicitly checked whether the buildup of the hot gas in halos changes with this additional physics and found no difference, i.e. the transition mass between cold gas and hot gas dominated halos is the same as in all the other simulations used in this paper. The gravitational softening in this simulation is  $220h^{-1}$  pc (Plummer equivalent) physical at  $z = 3$  and it increases to  $440h^{-1}$  pc physical at  $z = 1$ . Such high resolution is nec-

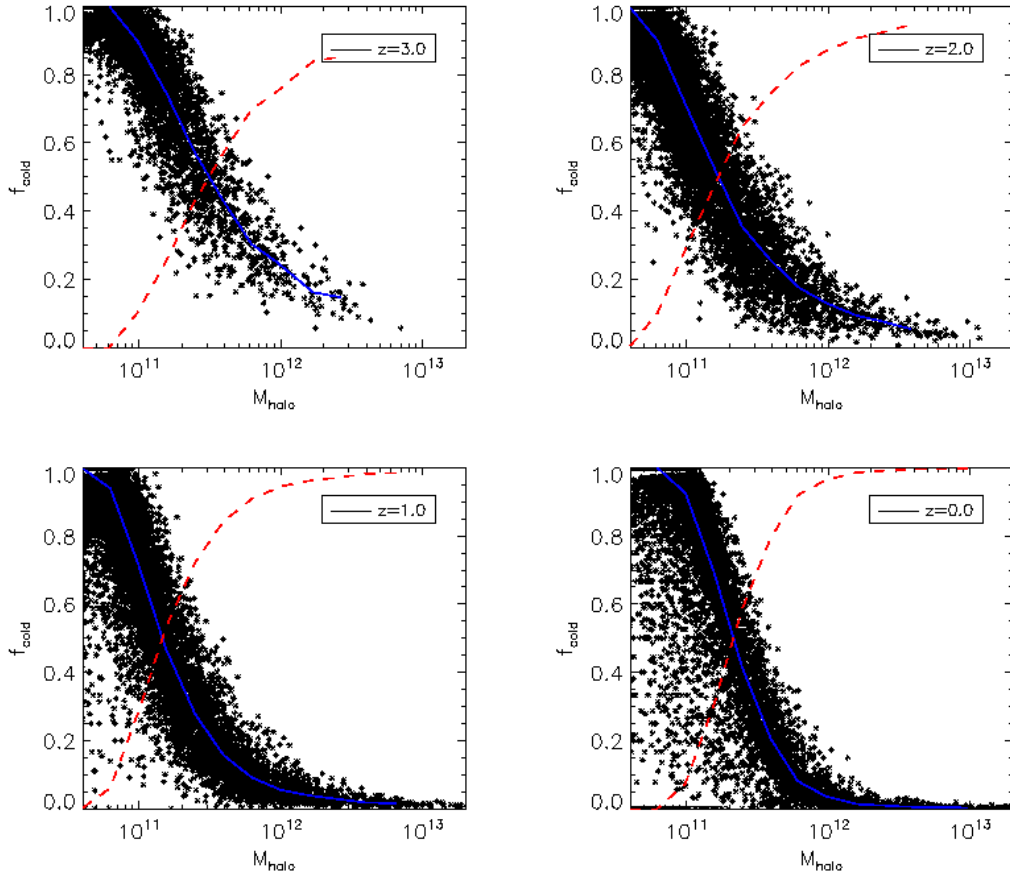


**Figure 3.** The fraction of cold halo gas in a halo of a given mass at four different redshifts. Lines show the running median of the cold gas fraction (blue, solid) and the hot gas fraction (red, dashed). (We exclude any galactic gas.)

essary to see the variety of structures in the cold accretion flows and to properly resolve the regions very close to the galactic disks.

Figure 4 shows the characteristic structure of cold mode gas in halos below the transition mass: a halo at  $z = 3$  with  $M_h = 1.1 \times 10^{11} M_\odot$  (upper panels) and a halo of the same mass at  $z = 1$  (lower panels). The particles are color coded by temperature, and their relative density on the plot indicates the projected column density (because the masses of the gas particles out of galaxies are usually identical). To illustrate the filamentary geometry, we show two different projections of each halo.

As emphasized in K05, owing to the presence of the dense filamentary streams, a typical high redshift halo has regions of great density contrast. High densities and short cooling times in these filaments make conditions unfavorable for shock propagation (Binney 1977; Binney & Dehnen 2003). In the inter-filamentary regions, where the gas density is often one or two orders of magnitude lower, some gas shock heats even when the halo mass is much lower than the transition mass. This is in contrast with simple 1D models, which necessarily average away density variation at a given radius, and which typically show a quick transition from cold mode to hot mode. In the upper panels of Figure 4, dense filamentary flows connect to the outskirts of the central galaxy and to an infalling satellite galaxy (see

§ 3.5). Tidal interaction has created a bridge between these two galaxies. Near  $R_{\text{vir}}$  the filaments are thicker than the galaxies themselves, but they are then compressed by the surrounding shock heated (virial temperature) gas, which extends to  $\sim 0.5 R_{\text{vir}}$ . Near the galaxies, the filaments are narrower than the galactic disks.

The situation changes at low redshift, where lower mass galaxies typically reside in larger filamentary structures comparable in cross section to the size of the halo. However, the densest parts of the filaments can still survive within the virial radius. Deeper in the halo, some of this gas gets shock heated to the virial temperature and some stays cold, resulting in a mixture of cold and hot accretion that supplies the gaseous galactic disk visible in the lower panels of Figure 4.

Figure 5 shows more massive halos, with mass  $M_h \approx 10^{12} M_\odot$ , a factor  $\sim 3$  above the transition mass seen in Figure 3. The limited volume of our L12.5/288 simulation does not contain any halo of this mass at  $z = 3$  so we show halos at  $z = 2$  and  $z = 1$ . Here the situation changes dramatically. At  $z = 2$ , a typical  $\sim 10^{12} M_\odot$  halo evolves at the intersection of several filamentary structures. The shock heated gas in this halo fills up the cavities between the filaments, and in some directions it extends to several virial radii. One can clearly see how gas that falls onto a halo from the region between the filaments gets heated at a shock front, typically

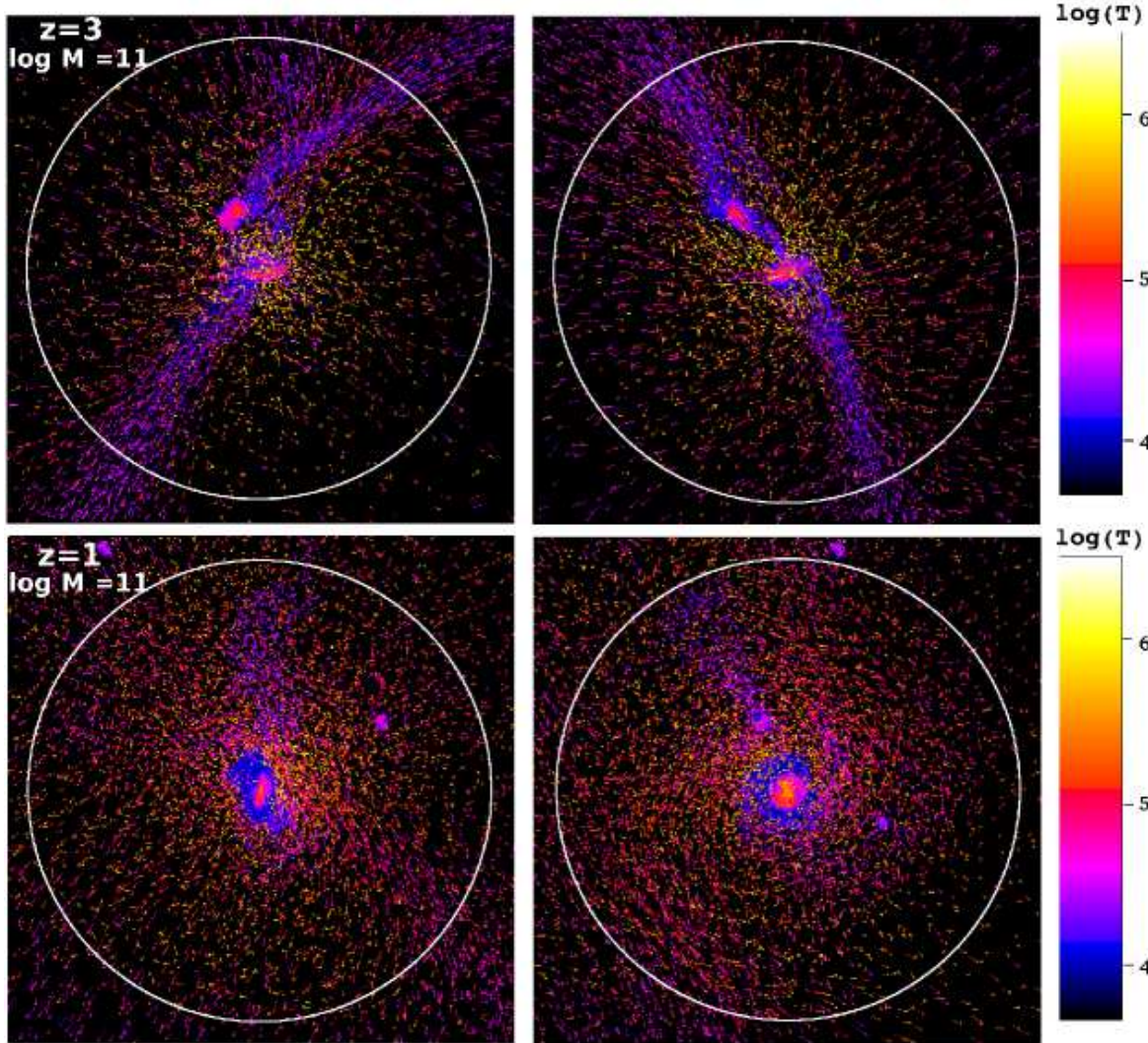


**Figure 4.** Temperature of the gas in low mass halos at  $z = 3$  and  $z = 1$ . Panels show the gas in a region of  $250h^{-1}$  kpc (comoving) on a side and  $250h^{-1}$  kpc (comoving) in projected depth. The virial radius is shown as the circles. Upper panels show the two different projections of a halo at  $z = 3$  dominated by a cold halo gas with  $M_h = 1.1 \times 10^{11} M_\odot$ , while lower panels show a halo at  $z = 1$  with  $M_h = 1.12 \times 10^{11} M_\odot$ . Vectors attached to particles show their projected velocities. Note that warmer gas temperature within the densest clumps is caused by sub-resolution implementation of the two-phase star forming medium.

slightly outside  $R_{\text{vir}}$ . The middle and the lower panels show only the gas with  $T < 10^5 \text{K}$ , to reveal the penetration and filamentary structure of the cold accretion. These filaments are enhanced by infalling substructures, which drags parts of the filaments into the more massive halos and often splits larger filamentary structure into multiple flows separated by hot gas. Furthermore, halos of this mass are dominated by hot gas at  $T \sim T_{\text{vir}}$ , which provides a high pressure environment that compresses the filaments. This results in the thin filamentary streams, most of which can penetrate to the halo's central regions. The zoom-in panel of the  $z = 2$  halo shows that these cold filaments survive to supply both the central and the satellite galaxies (in the upper right corner of this panel) with cold gas. However, a large fraction of the infalling gas is now shock heated to the virial temperature and fills the halo, so the accretion rate of the central galaxy in this halo is a factor of several below the halo accretion

rate. The filamentary streams in this panel show clumps and disturbances from substructure. The filaments dragged by the infalling substructure typically infall with a larger impact parameter bringing in large amounts of high angular momentum gas.

Results for the  $z = 1$  halo (right hand panel) are similar, but the incoming filaments are somewhat thicker compared to  $R_{\text{vir}}$  because a  $10^{12} M_\odot$  halo is no longer an unusually high density peak. At fixed overdensity, the physical density and cooling rates are lower, so a smaller fraction of cold filament gas survives its journey to the halo center, and more is shock heated to join the hot atmosphere.

In the most massive halo in our L12.5/288 simulation, with a mass of  $M_h \approx 9 \times 10^{12} M_\odot$ , the situation is different yet again as we show in Figure 6. In this high sigma peak, there are again multiple filaments entering the virial radius, and the inter-filamentary space is filled with shock heated

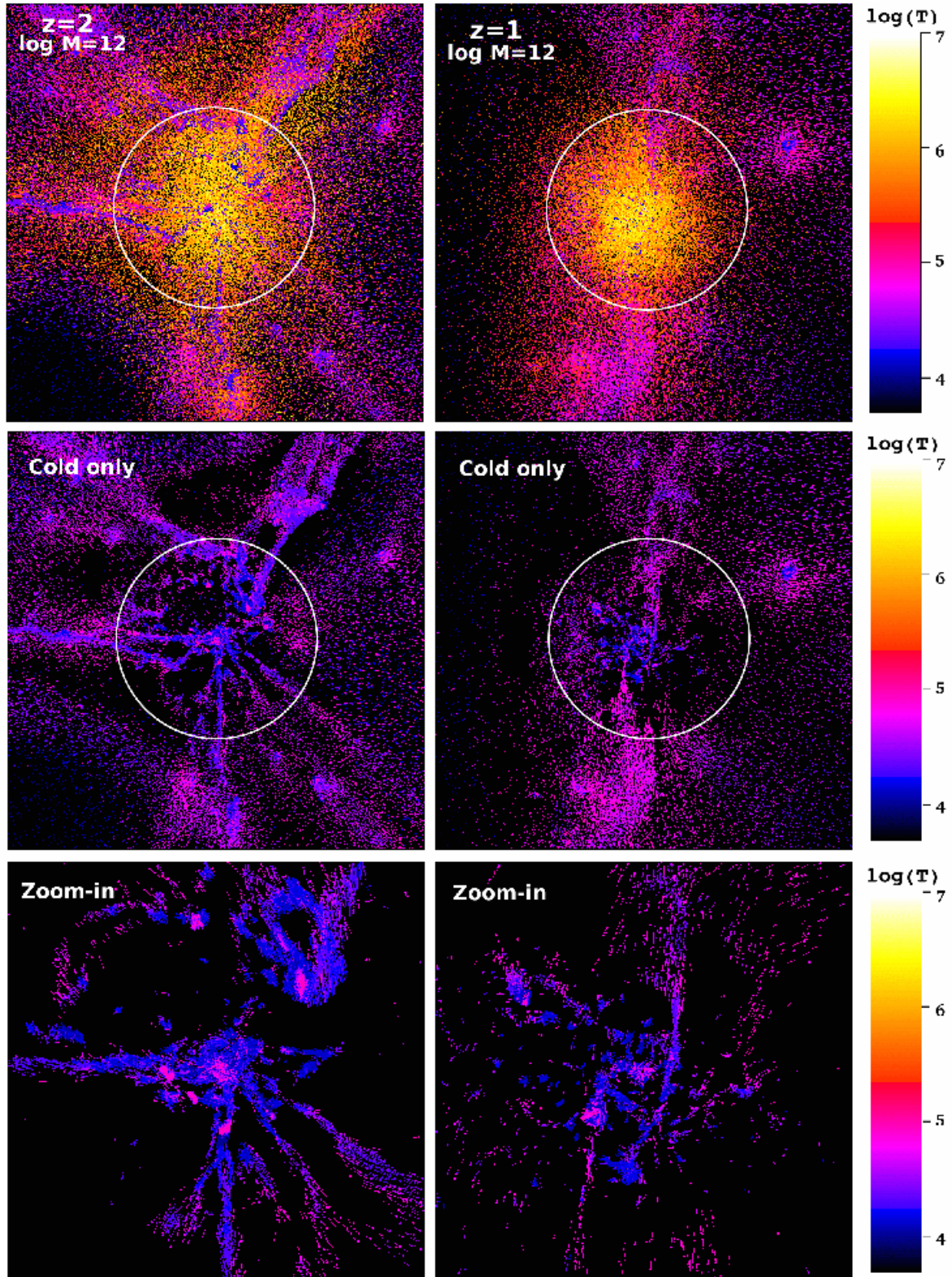


**Figure 5.** Temperature of the gas in Milky Way mass halos at  $z = 2$  and  $z = 1$ . Panels show the gas in a region of  $1h^{-1}$  Mpc (comoving) on a side and  $1h^{-1}$  Mpc (comoving) in projected depth. The virial radius is shown as the circles. Left panels show an  $M_h = 1.1 \times 10^{12} M_\odot$  at  $z = 2$ , while the right panels show an  $M_h = 1.2 \times 10^{12} M_\odot$  halo at  $z = 1$ . Upper panels show all gas particles. The middle panels show only the gas with  $T < 10^5 K$  but with the same color scale (indicated on the right). The lower panels also show only the low temperature gas, but are zoomed-in to show a region  $375h^{-1}$  kpc (comoving) on a side (approximately within  $0.8R_{\text{vir}}$ ) and  $125h^{-1}$  kpc (comoving) deep. Vectors attached to particles show their projected velocities. Note that warmer gas temperature within the densest clumps in middle and lower panels is caused by sub-resolution implementation of the two-phase star forming medium.

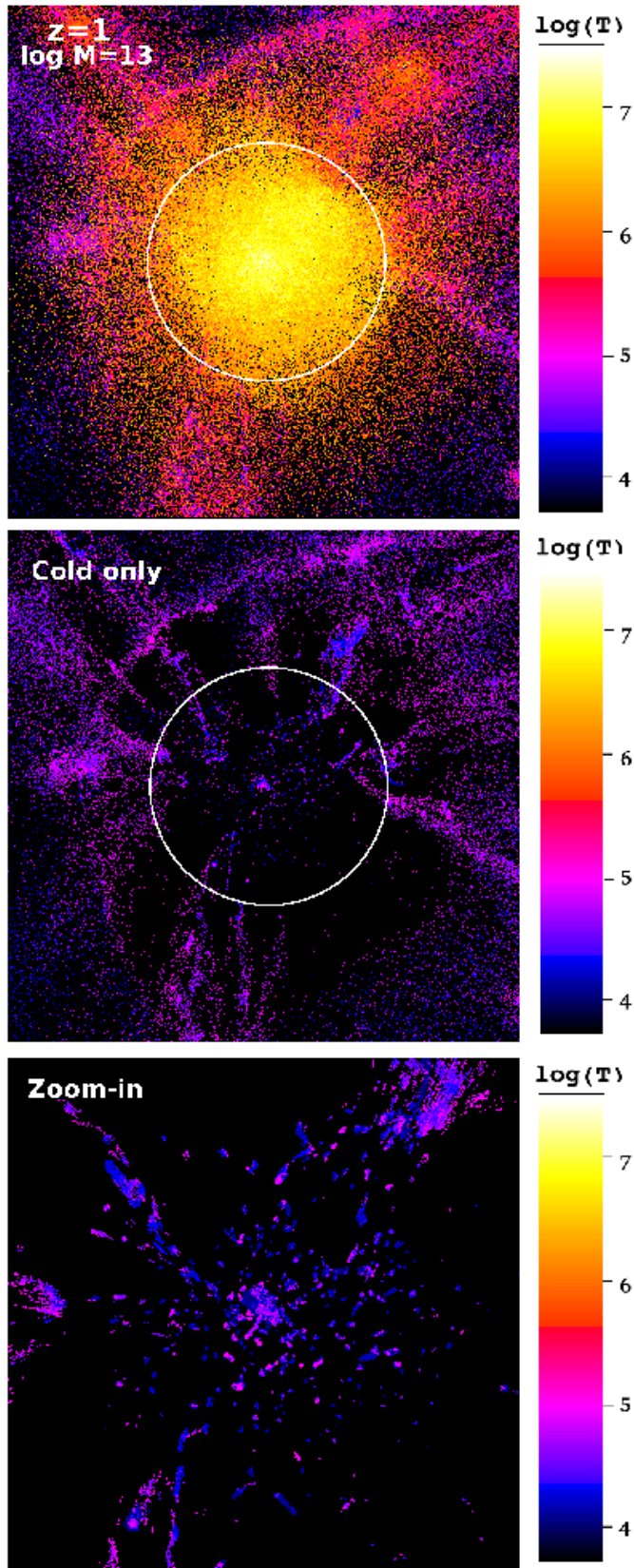


**Figure 6.** Temperature of the gas in a group size halo at  $z = 1$ , with  $M_h = 9 \times 10^{12} M_\odot$ . Panels show the gas in a region  $2h^{-1}$  Mpc (comoving) on a side and  $2h^{-1}$  Mpc (comoving) in projected depth. The virial radius is shown as the circles. Upper panels show all gas particles. The middle panels show only the gas with  $T < 10^5 K$  but with the same color scale (indicated on the right). The lower panels also show only the low temperature gas, but they are zoomed-in to show a region  $750h^{-1}$  kpc (comoving) on a side (approximately within  $0.8R_{\text{vir}}$ ) and  $250h^{-1}$  kpc (comoving) deep. Vectors attached to particles show their projected velocities.

gas that extends well beyond  $R_{\text{vir}}$ . Compressed by this hot medium, the filaments are even thinner compared to the virial radius. However, the middle and lower panels show that these cold flows do not penetrate deeper than about  $0.5R_{\text{vir}}$ . Some of the filaments are still connected to satellite galaxies, but the inner satellites and the central galaxy are separated from this gas supply. The bottom, zoom-in panel shows that the remnants of the filamentary flows clump into numerous dense cold clouds. Some of these dense concentrations of gas are actual galaxies, but most are a consequence of fragmentation of the filamentary flow induced by shocks and high pressure, cooling instabilities of the warm/hot gas, or clouds that form out of stripped galactic material. Accretion of such clumps can provide fresh gas for central galaxies in massive halos, at least in simulations without strong preventive feedback.

### 3.4 Accretion rates of individual galaxies

The accretion rates of individual galaxies as a function of their mass and of the central galaxies as a function of their parent halo mass are shown in Figure 7. We also plot the median accretion rates of the central galaxies as a solid line and the median accretion rates of satellite galaxies at a given mass as a dashed line (left panels). The larger simulation volume, compared to K05, allows us to highlight some details that were previously not very clear, especially for the high mass end at low redshifts, which we will discuss shortly.

At  $z = 4$  all the galaxies are completely cold mode dominated, and the accretion rates have a steep dependence on galaxy and halo mass. A typical  $10^{10}M_{\odot}$  galaxy and a typical central galaxy in a  $10^{11}M_{\odot}$  halo accrete at  $10 - 15M_{\odot}/\text{yr}$ , while galaxies in halos of around  $5 \times 10^{12}M_{\odot}$  accrete at  $30 - 100M_{\odot}/\text{yr}$ .<sup>3</sup> At  $z = 2$  galaxies at all masses are still cold mode dominated, but the dependence of the accretion rate on galaxy and halo mass becomes very shallow. For a change in halo mass of two orders of magnitude, from  $10^{11}M_{\odot}$  to  $10^{13}M_{\odot}$ , the smooth gas accretion rate of central galaxies increases by only a factor of  $\sim 2$ . The massive halos at  $z = 2$  are already full of hot virialized gas, and only a tiny fraction of this halo gas cools, resulting in the very low hot mode accretion rates. Between  $z = 2$  and  $z = 1$ , the median accretion rates at the low mass end drop by factors of  $\sim 2 - 3$ . Not only are the trends with mass now shallow, but above  $\sim 2 \times 10^{12}M_{\odot}$  the accretion rates of the central galaxies actually start to decrease with mass, though they turn up again above  $10^{13}M_{\odot}$ .

In the mass range where the accretion rates are decreasing with mass, the halos are full of hot virialized gas that cannot cool. At the highest mass end, where the gas accretion rates once again increase with mass, cold mode accretion dominates. In massive halos only the remnants of the cold filaments survive at low redshift, in the form of cold clouds. Some of these clouds are bound and identified with

<sup>3</sup> The typical accretion rates in Figure 7 are lower than those reported by Dekel et al. (2009) by a factor of several. However, they report total gas fluxes through to the inner 15 kpc of their simulated halos rather than the smooth gas accretion rates of their central galaxies; the difference between these quantities could be significant.

SKID, so we do not count them as smooth accretion even though they are not galaxies in the classical sense, i.e. they are not embedded in dark matter halos. Cold clouds not identified by SKID as galaxies also contribute to this cold mode accretion in massive halos. In addition, some cold, galactic gas gets decoupled from the stellar component owing to strong ram pressure and tidal forces.

The accretion of cold clouds with these various origins causes the cold mode accretion in very massive halos at late times. While part of this accretion could be realistic, much of it is probably a consequence of numerical artifacts, for the reasons discussed in §4.3 below. Since most of this accretion comes from clouds with masses slightly below the resolution limit (see §3.7), we refer to it as “cold drizzle”. Whether or not this cold drizzle is physical or numerical, the fact remains that group and cluster mass halos, which have masses at least an order of magnitude above the transition mass between cold and hot mode accretion dominated galaxies, effectively stop accreting gas from their hot virialized halos, i.e. the hot gas no longer cools.

The results at  $z = 0$  reveal some interesting trends. The dependence of the accretion rates on galaxy and halo mass are similar to  $z = 1$ , but the rates are lower overall. At the low mass end the rates increase from around  $0.2 - 0.3M_{\odot}/\text{yr}$  in halos with masses of  $\sim 10^{11}M_{\odot}$  to  $1 - 1.5M_{\odot}/\text{yr}$  in  $\sim 10^{12}M_{\odot}$  halos. Once again, the rates drop for masses above  $10^{12}M_{\odot}$ . At halo masses larger than several times  $10^{11}M_{\odot}$ , the halos are completely dominated by hot mode accretion, except for the most massive halos where potentially spurious cold drizzle provides several  $M_{\odot}/\text{yr}$  of accreted gas and where the hot mode rates are even lower. Most halos have lower accretion rates at  $z = 0$  than at  $z = 1$ , and smooth accretion is almost completely shut off in halos with masses larger than several times  $10^{12}M_{\odot}$ . However, there is a sizeable population of halos with masses of  $\sim 10^{12} - 5 \times 10^{13}M_{\odot}$  whose accretion rates have increased since  $z = 1$ , and the mass dependence of the upper envelope of accretion rates is quite steep. These halos have developed what could be considered classic cooling flows (Fabian 1994). In the same mass range, the majority of the halos have accretion rates, especially in the hot mode, that are very small. We will discuss the detailed properties and statistics of cooling and non-cooling halos in §4.

The left panels of Figure 7 also list the fraction of galaxies with extremely low accretion rates, less than 15% of the median accretion rate of galaxies at  $2 \times 10^{10}M_{\odot}$ . Specifically, we adopt thresholds of 0.1, 0.3, 1 and  $3M_{\odot}/\text{yr}$  at  $z = 0, 1, 2,$  and  $4,$  respectively. These galaxies typically accrete only one or zero gas particles between the two simulation outputs, and most such objects are satellite galaxies in larger parent halos.

### 3.5 Gas accretion in satellite galaxies

Figure 7 includes a comparison of central and satellite accretion rates in our GADGET-2, L50/288 simulation. At  $z = 4$ , the satellites and central galaxies have very similar accretion rates at a given galaxy mass. At  $z = 2$ , the satellites already accrete less than the central galaxies, but only a small percentage of galaxies have their accretion rates drastically reduced. The relative difference between central and satellite galaxies increases with decreasing redshift and is

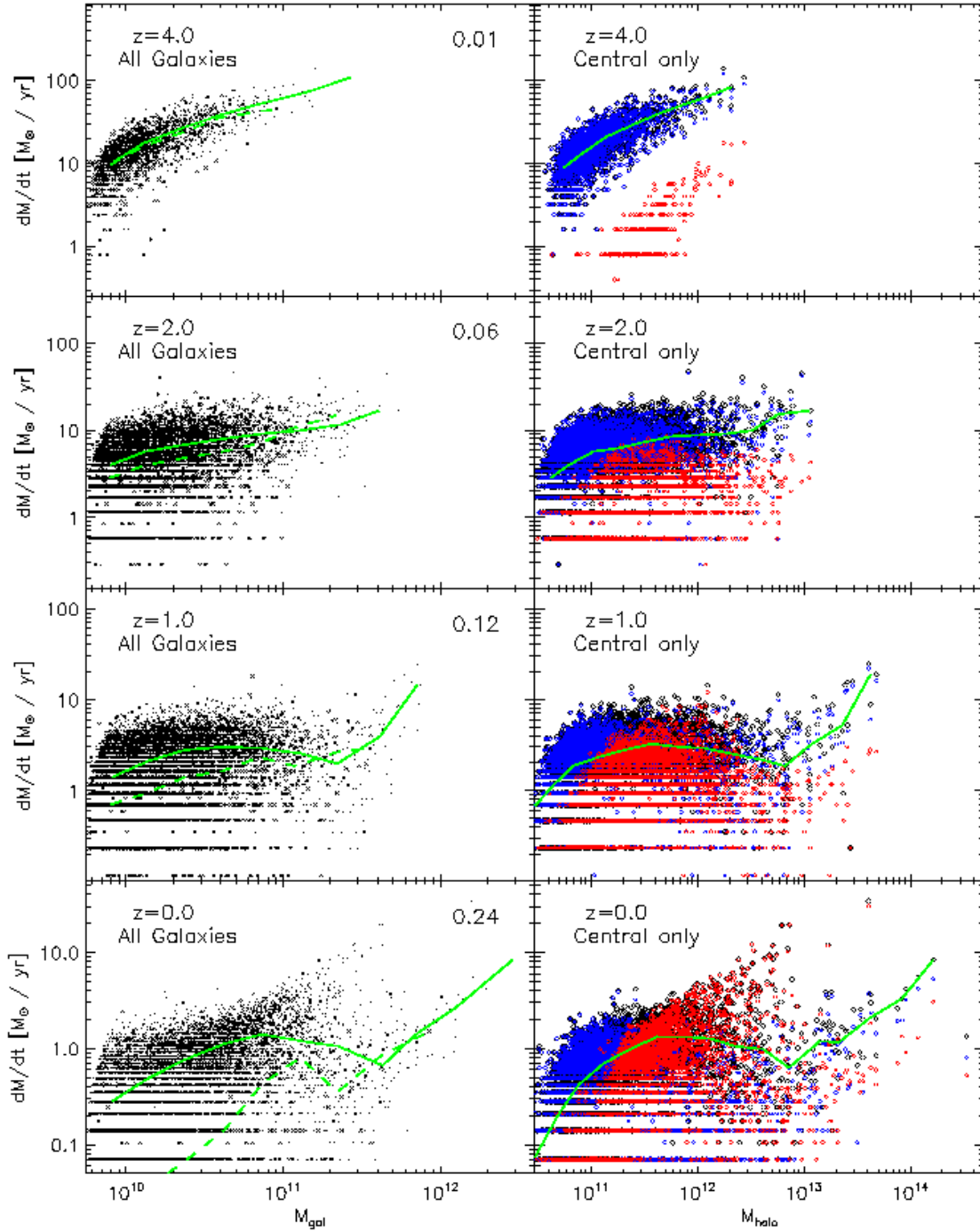


**Figure 7.** Smooth gas accretion rates of individual galaxies in the L50/288 simulation. In the left panels we show the accretion rates of all resolved galaxies as a function of their mass and in the right panels we show the accretion rates of the central (i.e. the most massive) galaxies in a given halo as a function of their parent halo mass. The satellite galaxies are marked with crosses, while the central galaxies are plotted as points in the left panels and diamonds in the right panels. In both columns, black symbols represent total accretion rates. In the right panels we also show cold mode accretion in blue and hot mode accretion in red. The solid line shows the median accretion rate of central galaxies at a given mass while the dashed line is for satellites. In the upper right corner of the left panels we also indicate the fraction of resolved galaxies with extremely low accretion rates (see the text for details). Note the different vertical scale for the  $z = 0$  panels.

quite large for lower mass galaxies at  $z = 1$ . At  $z = 0$ , the differences are substantial. The median accretion rate of the lowest mass satellite galaxies, those around the resolution limit, is zero. Note that owing to finite particle mass and the time interval between the two simulated outputs, we cannot measure accretion rates below  $0.07M_{\odot}/\text{yr}$ . However, even at  $z = 0$  around 45 percent of satellite galaxies are still able to accrete at rates above  $0.1M_{\odot}/\text{yr}$ . The differences in the accretion rates of higher mass satellites and central galaxies of equal mass decrease with galaxy mass, but they are still noticeable even in satellites with masses of  $\sim 2-3 \times 10^{11}M_{\odot}$ .

At any redshift, roughly 80% of the galaxies with extremely low accretion rates are satellites, except at  $z = 4$  where there is a roughly equal mix of satellite and central galaxies (but at this redshift the low accretion rate galaxies are only 1% of the total). The fraction of resolved galaxies with low accretion rates grows from 0.06 at  $z = 2$  to 0.12 at  $z = 1$  to 0.24 at  $z = 0$ . Although the median accretion rate of all galaxies is dropping over this interval, the increase in extremely low accretion rate galaxies is driven entirely by the growing gap between the central and satellite populations. This growing gap is also evident in the median rates — e.g., at  $M_{\text{gal}} \sim 2 \times 10^{10}M_{\odot}$ , the ratio of median accretion rates is a factor of  $\sim 2$  at  $z = 1$  and a factor of  $\sim 10$  at  $z = 0$ .

Simha et al. (2008) investigate the relative accretion and merger rates of satellite and central galaxies in the L22/128, P-TreeSPH simulation that is the main simulation analyzed by K05, and they discuss implications for the properties of central and satellite populations as a function of halo mass. Although the form of our analysis is different, the general trends here are consistent with those found in the more detailed investigation by Simha et al. (2008). In particular, despite the difference in simulation code, we find that a significant fraction of satellite galaxies have continuing gas accretion, and (in an investigation not illustrated here) that the satellites whose accretion is most strongly suppressed tend to be low mass systems in high mass halos. In addition, Keres (2007) analyzed satellite accretion in the cosmological simulations using P-TreeSPH, GADGET-2 and Gasoline (Wadsley et al. 2004) SPH codes and also found that the fraction of accreting satellites increases with increasing redshift and that the fraction of non-accreting satellites increases with increasing halo mass. These results are consistent with the view that satellites within the virial boundary of a halo may continue to grow by accreting gas from massive substructures in which they reside. These predictions (and the implied continuation of star formation in satellite galaxies) are supported by the empirical study of Weinmann et al. (2006), who find that satellite galaxies in the SDSS are less red than in semi-analytic models (SAMs) of galaxy formation. Especially at high redshifts, our simulation results indicate that the assumption commonly used in SAMs, that satellite galaxies stop accreting fresh gas as soon as they enter a larger halo (adopted by, e.g., Kauffmann et al. 1993; Cole et al. 1994; Somerville & Primack 1999; Hatton et al. 2003, and in subsequent models from these groups), is not valid. At low redshifts this approximation might be correct for the bulk of galaxies, but there seems to be a mass dependence on the effect of satellite strangulation, and a substantial fraction of satellites experience continuing accretion.

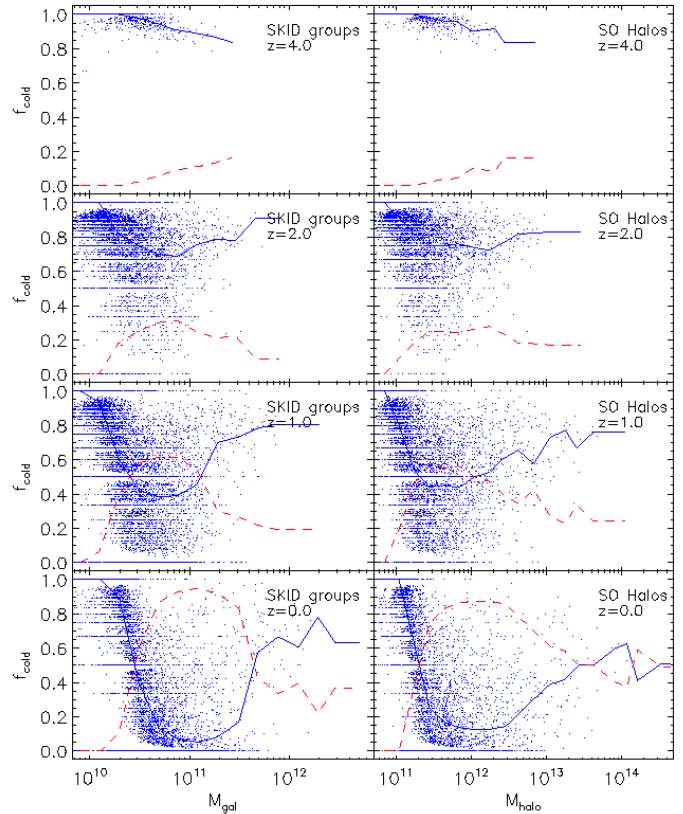


**Figure 8.** The fraction of total smooth gas accretion in cold mode (blue points) as a function of galaxy (left panels) and halo mass (right panels) at  $z = 4, 2, 1$  and  $0$ . The lines represent the median cold mode (blue, solid) and hot mode (red, dashed) fractions in a bin  $0.2$  dex in mass.

### 3.6 The fraction of accretion in cold and hot mode

The relative importance of hot and cold mode accretion is shown in Figure 8, where we plot the fraction of the total smooth gas accretion in these two modes as a function of galaxy and halo mass. At  $z \geq 2$  the accretion is dominated by the cold accretion mode at all masses. At  $z = 1$ , cold mode dominates at the low mass end, i.e. in galaxies with baryonic masses lower than  $2-3 \times 10^{10}M_{\odot}$  or halo masses lower than  $2-3 \times 10^{11}M_{\odot}$ . From  $M_{\text{halo}} \sim 2 \times 10^{11}M_{\odot} - 10^{12}M_{\odot}$ , cold and hot mode accretion are comparable on average. Above  $M_{\text{halo}} \sim 2 \times 10^{12}M_{\odot}$  cold mode once again dominates, but the spread in the cold accretion fraction of individual objects is very large. At  $z = 0$ , cold mode dominates at low masses, the hot mode begins to dominate at halo masses  $\geq 2-3 \times 10^{11}M_{\odot}$ , and it continues to dominate until masses of  $10^{13}M_{\odot}$ . Above this mass, the median cold and hot mode fractions are comparable, but the spread from halo to halo is very large. The significant cold mode fraction at high halo masses arises from a combination of very low hot mode accretion rates and “cold drizzle” (see §3.4), which may be mostly a numerical artifact. The absolute rates of cold accretion in these halos are still fairly small. We see that when a transition between cold and hot accretion occurs, the transition masses are  $M_{\text{gal}} \sim 2-3 \times 10^{10}M_{\odot}$  and  $M_{\text{halo}} \sim 2-3 \times 10^{11}M_{\odot}$ , very similar to the values in K05. However, the much lower hot accretion rates in the

GADGET-2 simulation changes the appearance of this plot relative to K05's figures 5 and 6: cold mode dominates at all galaxy and halo masses at high redshift, and at low redshift the hot mode domination at intermediate masses gives way to (possibly spurious) cold mode domination at the highest masses.

### 3.7 Star formation rates

In Figure 9 we show the star formation rates of the individual galaxies (on the left) and of the central galaxies in halos (on the right) as a function of the galaxy and halo mass. We plot the median star formation rate as a solid line and the median smooth accretion rate from Figure 7 as a dashed line. We also show the smooth gas accretion rates when we allow sub-resolution clumps to be counted as accretion (dotted) and the total gas accretion rates, which includes the gas supplied by mergers (dot-dashed). In addition we also show median of the total baryonic mass supply (i.e. including both gas and stars). In all four cases we exclude galaxies with zero star formation rate. The overall star formation rate follows the smooth gas accretion rate, but there are systematic deviations from this trend.

In low mass galaxies at low redshift, the typical gas accretion rates are higher than the star formation rates. The accreted gas in low mass galaxies needs to build up a sufficient reservoir before a significant fraction of the gas can cross the star forming threshold density. This physical effect is modulated by a numerical artifact: the gas densities in the central parts of these marginally resolved objects are underestimated, which delays the onset of efficient star formation until even higher masses. Because of this gas accumulation at the low masses, lower mass galaxies are always much more gas rich than their higher mass counterparts. As many low mass galaxies are indeed observed to be more gas rich at both low (Bell & de Jong 2000) and high redshift (Erb et al. 2006), part of this effect could indeed be physical, but the exact delay in star formation also depends on the resolution. The simulations with higher mass resolution show that this behavior shifts to lower masses as higher densities can be resolved, allowing the star formation rate to follow the gas accretion rate more closely.

Conversely, the star formation rates of high mass galaxies are typically higher than their accretion rates because of the larger contribution of minor and major mergers, which provide galaxies with gas as well as stars. In addition, the same objects usually have slightly higher gas accretion rates at earlier times, so the delay between accretion and star formation boosts the latter relative to the former. Comparison of the dashed and dotted lines also indicates that a large amount of the gas accretion in massive galaxies and halos comes from sub-resolution clumps (cold drizzle), which (as discussed previously) may be a numerical artifact. Below  $M_{\text{gal}} \sim 10^{11} M_{\odot}$  or  $M_{\text{halo}} \sim 10^{12} M_{\odot}$ , adding sub-resolution mergers to smooth accretion makes a negligible difference. The gas supply from resolved mergers appears to be only mildly important and only at the high mass end. Mergers do dominate the total mass buildup of massive galaxies (e.g. Maller et al. 2006) at late times but most of the mass they supply is in form of stars.

At all times galaxies form a well defined star forming sequence with mass, with a slope similar to the observed

slope (Daddi et al. 2007; Noeske et al. 2007). However, the normalization of the simulated relation is lower than that observed (see Davé 2008). Similar to the gas accretion rates, the typical star formation rate for central galaxies in Milky Way size halos ( $\sim 10^{12} M_{\odot}$ ) is  $\sim 2 M_{\odot}/\text{yr}$  at  $z = 0$  and grows to  $\sim 40 M_{\odot}/\text{yr}$  at  $z = 4$ , albeit with a sizeable scatter. The star forming sequence has less scatter as a function of galaxy mass than as a function of halo mass. This indicates that the galactic star formation law also plays a role in the regulation of this sequence, together with the main driver of gas supply, cold mode accretion. As we discuss in Paper II, reproducing the observed distribution of star formation rates in high mass galaxies requires that the gas accretion for most of these systems be sharply reduced but that a fraction of them retain the accretion and star formation predicted by the simulation.

### 3.8 Galaxy buildup

An intermediate or high mass galaxy may be dominated by hot accretion at  $z = 0$ , but it spent earlier phases of its growth below the cold-to-hot transition mass, and at high redshift where all galaxies are dominated by cold mode accretion. In addition, a massive galaxy may have grown partly by mergers with systems that were themselves built by cold mode accretion. Figure 10 shows the contribution of gas *initially* accreted through cold mode to the *final* masses of galaxies at  $z = 0$ . Here, we select all the particles that are contained in resolved galaxies at  $z = 0$  and trace their temperature history back through time. For each particle, we find the maximum temperature that it has ever reached before that redshift. We exclude any times when the particle's density was higher than the two-phase medium threshold in GADGET-2, to avoid counting temperatures that were increased through the sub-resolution star formation algorithm. If the temperature of the particle has never exceeded 250,000 K, we count it as being accreted through cold mode.

As expected, a typical low mass galaxy forms completely through cold accretion. The contribution of hot mode accretion increases until  $M_{\text{gal}} \sim 4 - 5 \times 10^{10} M_{\odot}$ , where the cold mode contribution is  $\sim 70 - 75\%$ , but then the trend reverses and the hot mode contribution starts decreasing in more massive galaxies. This reversal is caused by the increased contribution of low mass mergers and mergers at early times, which both add mostly cold mode accreted material to the massive galaxies. The near absence of hot mode accretion in massive halos reinforces this trend. The median cold mode contribution at masses  $M_{\text{gal}} \sim 5 \times 10^{11} M_{\odot}$  is higher than 90%, and it varies between 75% and 95% at even higher masses. The dispersion in the cold mode fraction is large at all masses. Removing ‘‘cold drizzle’’ does not alter our conclusion that even the most massive galaxies are built from baryons that were originally acquired via cold mode accretion.

The increase of the cold mode contribution at the highest masses is a consequence of ‘‘downsizing’’ in galaxy formation, whereby progenitors of the most massive galaxies today formed most of their stars and acquired most of their mass at earlier times than less massive galaxies. This trend is established by numerous observations, and while it is sometimes described as ‘‘anti-hierarchical,’’ it is predicted both by semi-analytic models and by numerical simulations based on the

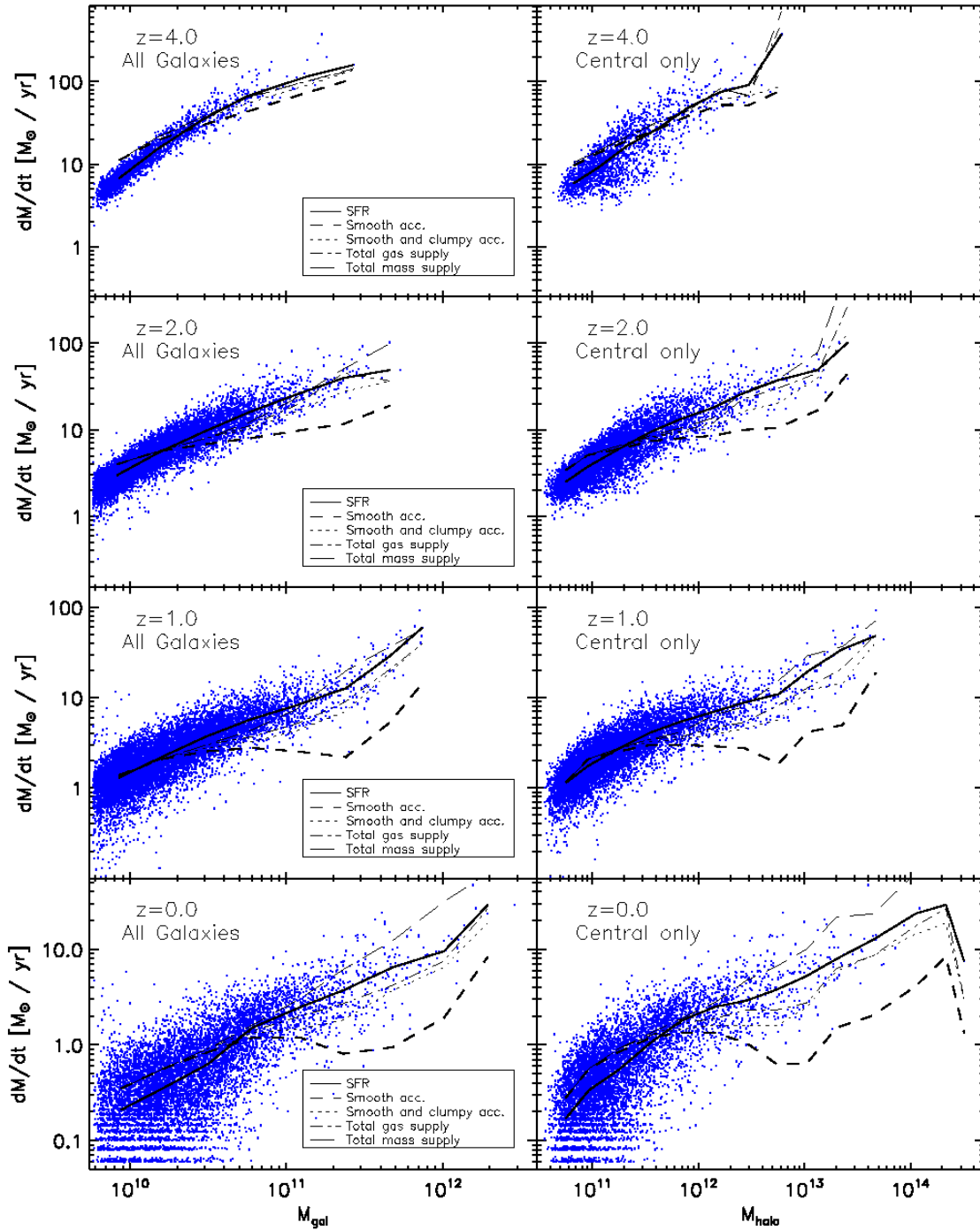


**Figure 9.** Star formation rates of individual galaxies in the L50/288 simulation. In the left panels we show the star formation rates of all resolved galaxies as a function of their mass and in the right panels we show the star formation rates of the central (i.e. the most massive) galaxies in a given halo as a function of the parent halo mass. The solid line shows the median star formation rates and the dashed line over plots the median smooth gas accretion rates similar to Figure 7. The dotted line shows the smooth gas accretion rate if we include sub-resolution clumps (see text for details). The dot-dashed line includes all channels of gas supply, smooth accretion, clumpy accretion and gas delivered through resolved mergers, while the long-dashed line also includes the supply of stellar component (mostly through mergers). The galaxies with zero star formation rates are excluded.

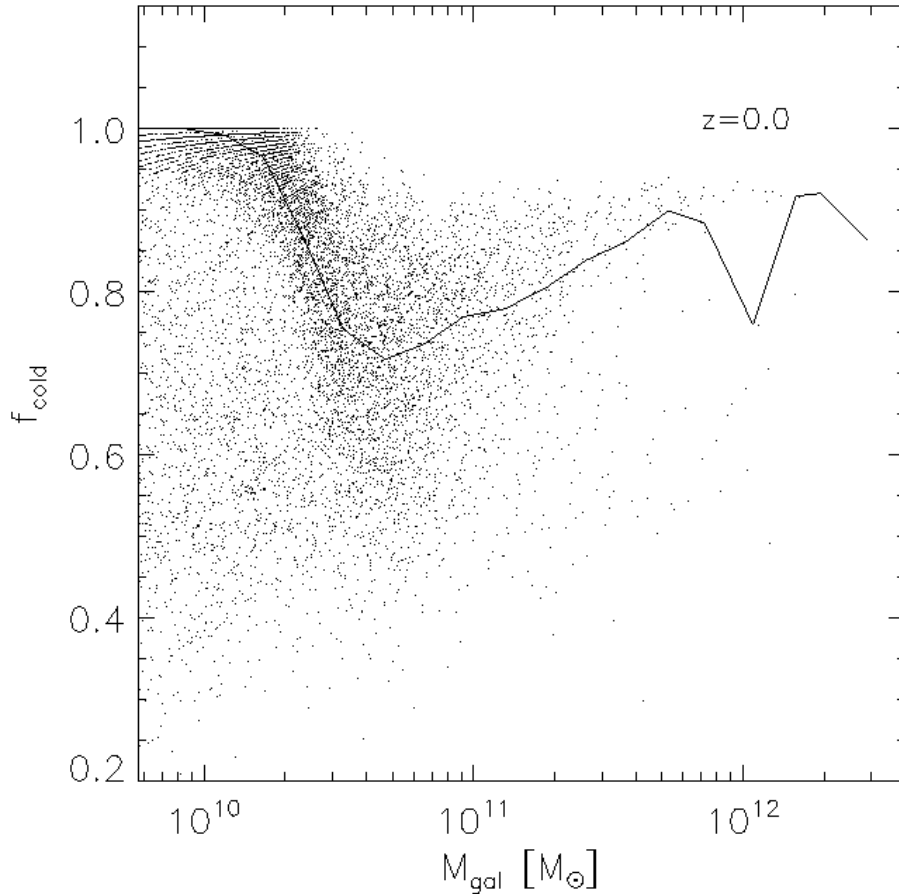


**Figure 10.** The fraction of galactic baryonic mass initially accreted through cold mode plotted as a function of galaxy mass at  $z = 0$ . The solid line plots the median fraction acquired through cold mode in bins 0.15 dex in mass.

$\Lambda$ CDM cosmology. We will discuss galaxy buildup in more detail in Paper II. However, it is clear from our results here that that owing to the high efficiency of cold mode accretion in lower mass objects, the low efficiency of gas cooling in massive halos, and the hierarchical buildup of the high mass objects, the typical galaxy at any mass assembles primarily through cold mode accretion. While important in some individual cases and in a limited mass range, cooling from the hot virialized atmosphere, as emphasized in the standard paradigm (Rees & Ostriker 1977; White & Rees 1978), represents only a secondary channel of galaxy growth. While feedback and metal cooling could increase cooling from the hot atmosphere, as discussed in the next section, these effects would also increase the mass range over which cold mode accretion dominates, as discussed in §3.2. We therefore expect this conclusion to hold even in simulations that include these processes.

### 3.9 Resolution effects

We briefly discuss the effects of resolution on our findings. For this purpose we use the L11/64 and L11/128 simulations (see Table 1), which have the same initial conditions

as the corresponding simulations in K05 but were evolved using the GADGET-2code. The mass resolution of L11/64 is comparable to our L50/288 simulation, while L11/128 has a factor of eight higher mass resolution (a factor of two in spatial resolution), including additional small scale power in the initial conditions. We compare these simulations only down to  $z = 1$ , since structure on scales larger than the simulation box becomes nonlinear at lower redshifts.

Comparing the galaxy mass function at masses that should be resolved by both simulations, at the low mass end the L11/128 simulation has a higher mass function while at the high mass end they both agree quite well. The smooth gas accretion rates in L11/128 relative to L64 are around 30 percent lower for most halo masses, over the whole redshift range. The same applies to the star formation rate. These lower rates owe to the higher resolution, which enables lower mass objects to form at earlier times, converting part of their gas supply into stars and hence lowering their gas accretion rates at a given redshift. With higher resolution the star formation in any galaxy also begins earlier because higher gas densities can now be reached, and it therefore locks more baryons into stars at a given time, again decreasing the amount of gas available for star formation at later times.

Owing to the small volume, there are only two halos more massive than  $3 \times 10^{12} M_{\odot}$  at  $z = 1$  in the L11 simulations. In the case of central galaxies in these two halos, differences in the star formation rate are quite small at  $z \gtrsim 2$  but increase to 30-40 percent by  $z = 1$ . The cooling of hot gas in massive halos is very inefficient in both simulations, but it is even less efficient in L11/128, which is not surprising as a slightly larger fraction of baryons are now locked up in galaxies. The effect of “cold drizzle” from the sub-resolution objects, which dominates the supply of gas to massive galaxies at late times, is similar at high resolution if we count only accretion below the  $64 \times m_{SPH,L11/128}$  threshold, but it is significantly less pronounced in the higher resolution simulation if we count the gas accretion from groups below  $64 \times m_{SPH,L11/64}$ . This result remains the same even if we account for the gas contribution from resolved mergers (as some of the cold clouds are now above the resolution threshold), implying that there is a significant decrease in the total accretion of cold gaseous clouds in the higher resolution simulations. At least part of this effect must owe to the fact that galaxies of a given mass are actually more gas poor in the higher resolution simulations, and there is therefore less gas available for stripping once they fall into a massive halo, but it could also suggest that the evolution of the cold clumps is greatly affected by our limited resolution. We also find that the typical mass of the cold gas clumps in the halo are lower in the higher resolution simulation.

The L11/64 vs. L11/128 comparison suggests that our conclusions about the declining importance of hot mode accretion in massive halos would if anything be stronger at higher resolution. They also indicate the robustness of our qualitative conclusions about the feedback mechanisms needed to reproduce observed galaxy masses and specific star formation rates, which is the subject of Paper II. The significant resolution dependence of the accretion and star formation rates for the most massive galaxies implies that the simulation results for these galaxies should be interpreted with caution. In particular, these tests provide some evidence that continuing cold accretion in the most massive galaxies at late times, is partially a numerical artifact, a point we return to in §4.3 below.

#### 4 COOLING AND NON-COOLING HALOS

In this paper, as in K05, we find that galaxy growth in halos below  $M_{\text{halo}} \sim 3 \times 10^{11} M_{\odot}$  is dominated by cold accretion, and that dominant hot gas components develop only above this mass. The important difference relative to K05 is that the hot mode accretion rates in these massive halos are much lower. The sign of this difference is as expected given the difference in SPH algorithms used, with the entropy-conserving algorithm providing a better separation between the cold and hot gas phases. However, as we show below, the cooling rates in most of our simulated massive halos are much lower than predicted by typical semi-analytic calculations in the absence of feedback. Furthermore, the range of cooling rates is large at fixed halo mass. In this section we discuss the origin of this large dispersion of cooling rates, the nature of the continuing cold accretion in high mass halos, and the possible connections to the observed properties of X-ray groups and massive galaxies.

#### 4.1 Gas profiles: cores and cusps

The right panels of Figure 7 show the accretion rates of central galaxies, and here we focus on the behavior at high halo masses. Above  $10^{13} M_{\odot}$ , there are 63 halos at  $z = 0$  and 28 halos at  $z = 1$ ; at  $z = 2$  we lower the threshold slightly to  $8 \times 10^{12} M_{\odot}$  to improve statistics, yielding 3 halos. At  $z \geq 1$  there is no clear demarcation between cooling and non-cooling halos, but if we take an arbitrary division at  $3.5 M_{\odot} \text{ yr}^{-1}$ , then 100, 65, and 13 percent of the massive halos are above this threshold at  $z = 2, 1,$  and  $0$ , respectively. If we consider only hot accretion, these percentages change to 33, 0, and 3.

Figure 11 compares the density and temperature profiles of two massive ( $M_{\text{halo}} \sim 4 \times 10^{13} M_{\odot}$ ) halos at  $z = 0$ , one in which the central galaxy has a high hot mode accretion rate of  $30 M_{\odot} \text{ yr}^{-1}$  and one with a (more typical) hot mode accretion rate of  $0.3 M_{\odot} \text{ yr}^{-1}$ . We only show particles that are part of a halo but are not part of the individual galaxies within a halo. The density profiles (shown by plotting the densities of individual SPH particles vs. radius) are strikingly different: the cooling halo has a roughly power-law profile in to  $0.01 R_{\text{vir}}$ , while the non-cooling halo has a core (more accurately, a sharp break to a shallower power law) inside  $\sim 0.15 R_{\text{vir}}$ . The temperature of the hot gas is roughly constant in to  $0.01 R_{\text{vir}}$  in the cooling halo, but in the non-cooling halo it rises by about a factor of two from  $R_{\text{vir}}$  to  $0.02 R_{\text{vir}}$ , inside of which essentially all gas particles are cold and belong to the central galaxy. These density and temperature profiles are typical of other high mass halos in these two regimes.

The right panels of Figure 11 show the instantaneous cooling times of gas particles in the two halos. In the cooling halo, particles out to  $0.1 R_{\text{vir}}$  have typical cooling times below  $10^{10}$  years. In the non-cooling halo, only a small fraction of particles have cooling times below  $10^{10}$  years. We can predict hot mode accretion rates from these plots by taking the amount of gas that can cool during the typical time between simulation outputs ( $\sim 1.3 \text{ Gyr}$  at  $z \sim 0$ ) and dividing by the time interval. We obtain  $36 M_{\odot} \text{ yr}^{-1}$  and  $0.17 M_{\odot} \text{ yr}^{-1}$ , in comparison to the measured hot accretion rates of  $30 M_{\odot} \text{ yr}^{-1}$  and  $0.35 M_{\odot} \text{ yr}^{-1}$ . Thus, the difference in hot mode accretion rates can be understood as a direct consequence of the difference in density and temperature profiles. While dynamical processes like shocks, infall, dynamical friction and turbulent motions likely contributed to the formation of cored profiles (e.g. Conroy & Ostriker 2008; Dekel & Birnboim 2008; Khochfar & Ostriker 2008), and they may have injected heat that offset cooling in the earlier stages of halo formation, at late times the simple “instantaneous” estimate of cooling can explain the very low accretion rates found in §3 without the need for any additional heating processes. We briefly checked the higher redshift results and found that similar cores start to form in the most massive halos in our simulation even at  $z = 2$ , albeit with slightly higher central densities. We will explore the profiles of the higher redshift sample in future work.

The density and temperature profiles of these two halos are reminiscent of the gas profiles in observed cooling flow and non-cooling flow clusters (e.g. De Grandi & Molendi 2002; Morandi & Ettori 2007). This leaves the question of what creates the range of profiles in the first place. In the

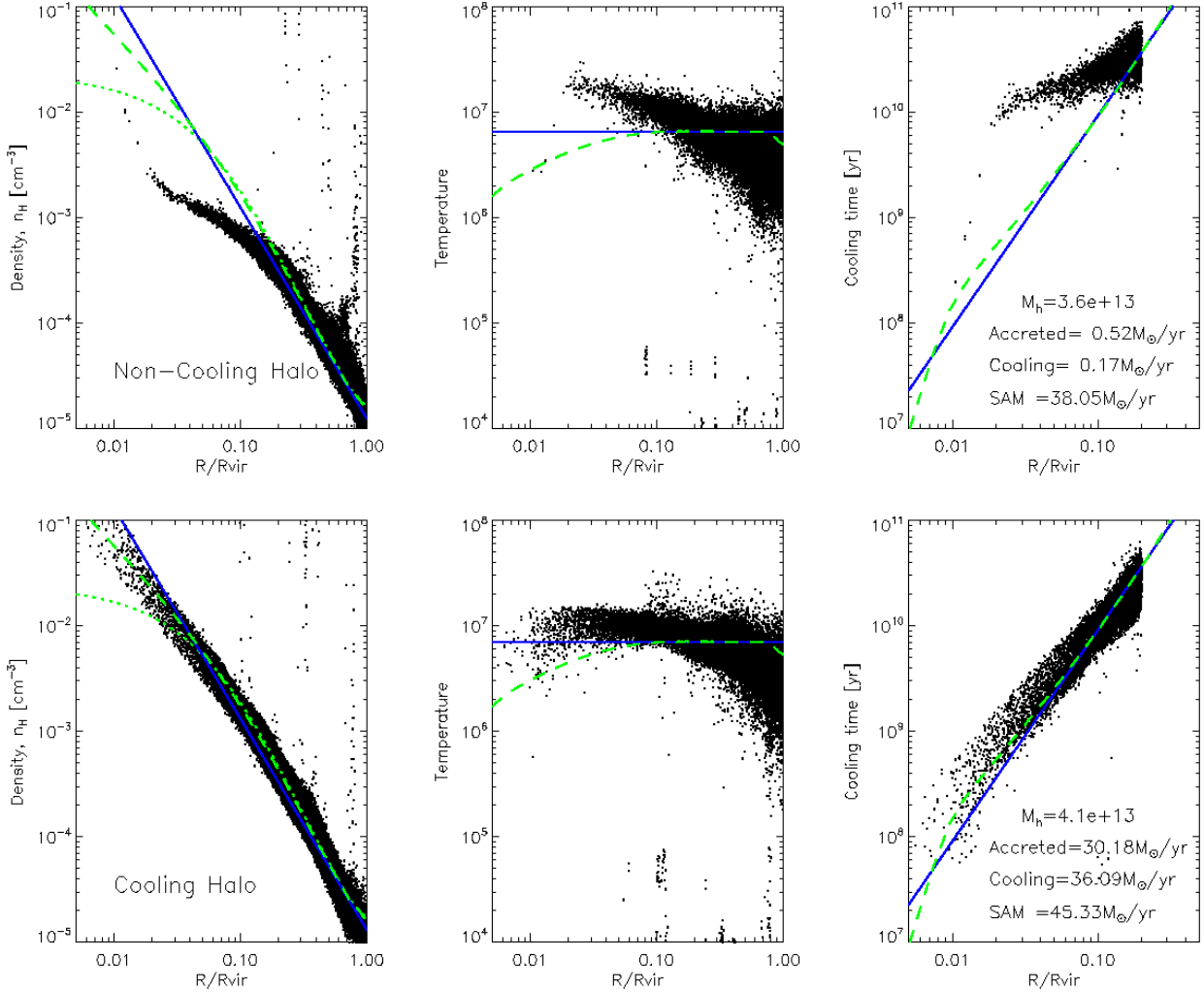


**Figure 11.** The gas properties at  $z = 0$  of two group size halos with masses of  $4 \times 10^{13} M_{\odot}$ , one that is not cooling as is typical (upper panels) and a rarer one that can cool (lower panels). The left panels plot the densities of gas in the halo (points). Model profiles are shown for an isothermal gas density (solid line) and the density calculated assuming an isothermal gas in hydrostatic equilibrium within an NFW potential for a  $10^{14} M_{\odot}$  halo, where dotted line shows the initial density profile and dashed line shows the gas density profile after it cools for 2 Gyr. The middle panels plot the gas temperatures and the right panels plot the gas cooling times. The right panels also indicate hot mode accretion rates from the simulation, an accretion rate from a simple cooling calculation, and the cooling rates from the SAM used in Croton et al. (2006) (see text for details).

cluster context, a common hypothesis is that mergers disrupt the quiescent gas evolution that would otherwise produce cooling flows. Large scale shocks during major mergers can raise the central entropy of the gas, thereby lowering the central density and increasing cooling times. As a rough test of this hypothesis, we compared the mean assembly redshifts (defined as the redshift at which the stellar mass of the largest progenitor exceeded half the mass of the  $z = 0$  galaxy) of the central galaxies of massive  $z = 0$  halos with hot mode accretion rates above and below  $3.5 M_{\odot} \text{ yr}^{-1}$ . These assembly redshifts indicate the time at which the central parts of the halo were largely in place. While the scatter is large and the number of systems rather small, we find that for  $M_{\text{halo}} > 8 \times 10^{12} M_{\odot}$  the mean assembly redshift of cooling halos is  $z \approx 1.7$ , while for non-cooling halos it is slightly below  $z = 1$ . Thus, it appears that halos with

a long quiescent phase after the assembly of their central regions are most able to build cuspy density profiles that allow substantial cooling (see also Burns et al. 2008). This can be understood from the buildup of the dark matter halos. The formation of dark matter halos proceeds in two stages, a rapid growth by major mergers at early times and slow growth by minor mergers at late times (Li et al. 2007). The time when the rapid growth stage finishes increases with increasing halo mass. While a large fraction of halos in the range of  $10^{12} - 10^{13} M_{\odot}$  typically still experience major mergers around  $z = 1$ , most such halos have finished their rapid growth by  $z = 0$ . For more massive halos, however, a significant fraction are still experiencing major mergers at  $0 \leq z \leq 1$ , though others are already in a stage of more quiescent growth.

In this scenario, cooling flows set in when the growth of

halos slows. Observationally, this view is supported by the study of Vikhlinin et al. (2007), who find that none of the  $\sim 20$  clusters they observe in X-rays at  $z > 0.5$  show any signature of strong cooling flow profiles. At low redshift, however, roughly half of the clusters in their sample have cooling flow profiles. In the bulk of clusters in their higher redshift sample, they also find some signatures of recent merger activity, and they conclude that the higher frequency of major mergers at higher redshifts is responsible for the difference in cooling flow fractions. In our simulation, we find no high mass halos with hot accretion rates above  $3.5M_{\odot} \text{ yr}^{-1}$  at  $z = 1$ . Cold accretion would not produce X-ray emission, so it is not relevant to this comparison. At  $z = 0$ , 3 percent of the  $M > 10^{13}M_{\odot}$  halos have hot accretion rates above  $3.5M_{\odot} \text{ yr}^{-1}$ , and 17 percent above  $1M_{\odot} \text{ yr}^{-1}$ . The fraction of cooling flows is thus low compared to the observations, but the redshift trend is correct. The predictions are likely to depend on halo mass as well as redshift, so quantitative comparison to data will require larger volume simulations with more halos in the mass range ( $\sim 10^{14} - 10^{15}M_{\odot}$ ) probed by X-ray cluster observations.

Our preliminary tests of simulations with stellar wind feedback and metal cooling from Oppenheimer & Davé (2006) show that even with the larger fraction of gas in these halos, gas density cores are still common in a mass range similar to that in our simulation. The central parts of these cores are able to cool at slightly higher rates than in our no-wind, no metal simulations. Despite the low cooling rates of our present simulations, additional feedback in group mass halos might be needed to keep their massive central galaxies red enough to match the observations. However, the formation of a gas density core that prevents or at least significantly slows down cooling from the hot atmosphere appears to be a generic result of hierarchical structure formation, even without feedback from AGN or other astrophysical sources. The exact fraction of halos affected, with or without additional feedback mechanisms, remains an open question.

## 4.2 Implications for Semi-Analytic Modeling

Returning to Figure 11, the solid blue lines show singular isothermal sphere (SIS) gas profiles,  $\rho \propto r^{-2}$ , scaled to the virial mass and gas fraction of these halos. This density profile describes the cooling halo fairly well, but it drastically overestimates the density inside  $0.1R_{\text{vir}}$  for the non-cooling halo. The solid green curve shows the density profile for isothermal gas in hydrostatic equilibrium in the profile of an NFW halo (Navarro et al. 1997) with the concentration expected for  $10^{14}M_{\odot}$  (Bullock et al. 2001), again scaled to the virial mass and gas fraction of our simulated halos. We modify the NFW potential to include the gravitational force softening at small radii, and this modification produces the flattening of the density profile inside  $\sim 0.05R_{\text{vir}}$ . In Keres et al. (2009b, in preparation), we evolve spherically symmetric gas distributions with these initial profiles using GADGET-2. The dashed green curve shows the density and temperature profile after the isothermal NFW distribution has been evolved (with cooling) for 2 Gyr. The evolved density profile approximately follows the SIS curve, while the temperature profile drops inside  $\sim 0.03R_{\text{vir}}$ .

The piecewise cooling solution of Bertschinger (1989) provides accurate estimates of the gas accretion rates at halo

center for profiles such as these (Keres 2007). Semi-analytic models frequently use an approximation to this solution, assuming either SIS profiles or isothermal gas in equilibrium in an NFW halo, to calculate accretion rates in massive halos. Comparing the cooling time profiles in Figure 11, it is clear that this approach will be reasonably accurate for the cooling halo but will overestimate the accretion rate in the non-cooling halo drastically. As a specific example, we applied the cooling algorithm used in the Croton et al. (2006) semi-analytic model: assuming an isothermal gas distribution and the gas fraction of the simulated halos, we calculate the accretion rate as  $dm_{\text{cool}}/dt = 0.5m_{\text{gas}}r_{\text{cool}}V_c/R_{\text{vir}}^2$ , where  $r_{\text{cool}}$  is defined as  $t_{\text{cool}}(r_{\text{cool}}) = R_{\text{vir}}/V_c$ . (We ignore the small difference in virial radius definition.) The predicted accretion rates are  $45M_{\odot} \text{ yr}^{-1}$  for the cooling halo, which is accurate at the 50% level, and  $38M_{\odot} \text{ yr}^{-1}$  for the non-cooling halo, which is more than two orders of magnitude above the actual accretion rate in the simulation. More detailed comparison of the simulation results to a full range of semi-analytic models will be presented elsewhere (Lu et al. 2008).

It is possible that the cores found here in most high mass halos are enhanced by some numerical artifact caused by the effective “phase separation” between hot and cold gas that arises in the entropy-conserving formulation of SPH. However, our tests on idealized cooling flow models (Keres 2007) suggest that GADGET-2 gives reasonably accurate results for halo masses and particle numbers like those considered here (more accurate than the codes without the entropy conserving SPH formulation). Taking the numerical results at face value, there are significant implications for semi-analytic models, since with standard assumptions they would greatly overestimate the cooling rates for the majority of high mass halos in this simulation. Some models reset their cooling radius after a major merger (e.g. Somerville & Primack 1999), which goes in the right direction, but an isothermal post-merger gas profile still leads to an overestimate of the cooling rates, by an amount that depends on the time interval and the algorithm used for the cooling calculation. Models that assume that there is a core in the gas density profile of massive halos (e.g. Bower et al. 2006) could in principle provide a better match to the central parts of our simulated halos, but the central temperatures in such models should also be increased to match the simulated gas properties. Moreover, models that assume a density core in *all* halos fail to represent the cooling flow systems that develop at late times. If semi-analytic models are consistently overestimating gas cooling rates in massive halos, then they are likely requiring too much feedback in these halos to compensate. More accurate calibration of the cooling recipes in semi-analytic models can be developed by comparing the evolution of gas profiles in hydrodynamic simulations and the semi-analytic calculations; the short analysis here provides a first step in this direction.

## 4.3 Cold Drizzle

Even at high halo masses and low redshifts, accretion onto central galaxies is usually dominated by cold gas in sub-resolution clumps, the form of accretion that we have described as “cold drizzle.” Thermal instability can form cold clumps *in situ* from hot halo gas (Mo & Miralda-Escude 1996; Maller & Bullock 2004), but the cold drizzle gas in

our simulations has *never* been hot, so thermal instability clouds are not its source. (Our simulation probably lacks the resolution needed to model thermal instability in galaxy mass halos in any case.) Rather, the cold drizzle appears to be a mix of gas that has been stripped from larger galaxies and sub-resolution clumps that form within cold/warm filaments that are disrupted at the outskirts of high mass halos, where they may be compressed by the surrounding hot gas.

Both of these sources should produce cold gas that can accrete onto galaxies in massive halos. However, there are several numerical effects that could artificially amplify this form of accretion in our simulation, perhaps by large factors. First, ram pressure stripping of cold gas from infalling galaxies (Gunn & Gott 1972) is almost certainly overestimated at the resolution of L50/288 because the typical smoothing lengths of the hot particles greatly exceed the size of the galaxies themselves (see tests and discussion by Tittley et al. 2001). Second, a similar effect could cause cold gas clumps (regardless of origin) to sink to the center of the halo more quickly than they should, as artificial ram pressure slows their tangential velocities. Finally, SPH codes have difficulty following surface instabilities that should develop when cold dense clumps move through a hot dilute medium (Agertz et al. 2007), so clouds that should be destroyed by instabilities or by conduction (which is not included in our simulations) may artificially survive their journeys to the halo center. As discussed in §3.9, we find that the amount of cold drizzle in massive halos at  $z = 1$  is reduced when the mass resolution is increased by a factor of eight relative to that of L50/288, though the limited redshift range and box size of our resolution tests does not allow us to draw clear conclusions about the influence of resolution on cold accretion rates in massive halos. In a systematic comparison of simulations run with different codes from the same initial conditions (Keres 2007), we find more cold drizzle in massive halos in simulations run with GADGET-2 compared to those run with PTreeSPH and Gasoline. This difference suggests that the effects mentioned above may be more severe for the GADGET-2SPH formulation because of the different calculation of the hydrodynamic forces and the different averaging of the properties of gas on the interface between the dense cold phase and the hot dilute medium, which could result in different rates of cloud survival and formation and different ram pressure forces at moderate resolution.

Our findings on low accretion rates in massive halos are qualitatively similar to those of Naab et al. (2007), based on much higher resolution GADGET-2 simulations of the formation of individual galaxies in a cosmological context. Like the simulation analyzed here, the Naab et al. (2007) simulation incorporates a simple star formation algorithm and has no strong feedback in the form of supernova-driven winds or AGN heating. At their highest resolution, Naab et al. find that the central galaxy in a halo of several times  $10^{12}M_{\odot}$  stops forming stars and is not supplied with new gas after a redshift  $z \approx 1$ ; thus they, too, find that accretion from the hot gas halo shuts off without the assistance of feedback. In their lower resolution simulations, however, accretion continues at lower redshift, perhaps in the form of cold drizzle like that in our simulations. Increased resolution could suppress this cold accretion both by more accurately treating ram pressure and instabilities and by depleting the gas sup-

ply in low mass clumps (which get converted into stars when the resolution is high enough).

We remain uncertain whether the cold accretion rates in massive halos in our simulation are approximately correct or substantially overestimated because of finite resolution and numerical effects in the GADGET-2SPH formulation. We show in Paper II that cold drizzle makes only a small contribution to the final masses of galaxies in these high mass halos, but it can significantly affect their star formation rates and hence their colors.

#### 4.4 A Natural End to Smooth Accretion?

Following the results of Katz et al. (2003) and Birnboim & Dekel (2003) on cold and hot accretion, several authors noted that simulations or semi-analytic models of galaxy formation would better reproduce observations of the galaxy luminosity function and the low star formation rates of massive galaxies if hot accretion were suppressed (Binney 2004; K05; Dekel & Birnboim 2006; Cattaneo et al. 2007). Motivated in part by observations of galaxy clusters, these authors and others suggested that preventive feedback from AGN might preferentially suppress hot accretion, since relative to cold accretion the hot gas has lower density, higher temperature, and larger geometrical cross-section. In one concrete implementation of this idea, Cattaneo et al. (2006) and Cattaneo et al. (2008) show that a semi-analytic model that assumes the shut-down of accretion and star formation in halos above a critical mass  $M_{\text{halo}} \sim 10^{12}M_{\odot}$ , together with traditional semi-analytic model assumptions about stellar feedback, reproduces many of the observed features of the galaxy red sequence and bimodality of the galaxy population. The semi-analytic models of Croton et al. (2006) and Bower et al. (2006) allow AGN feedback to suppress gas accretion in halos that, according to the cooling radius criteria in these models, have developed quasi-static hot gas halos (White & Frenk 1991), and these models also achieve better agreement with observations than earlier generations of semi-analytic models.

In this paper we find that the hot accretion rates in simulated massive halos are low even without any strong feedback mechanisms, principally because of the formation of cored gas density profiles that have long central cooling times. If we assume that cold drizzle in massive halos is mostly a numerical artifact that would disappear at high resolution (§4.3), we conclude that the physics of hierarchical halo assembly and galaxy formation on its own leads to a shutdown of gas accretion in massive halos. Naab et al. (2007) emphasize that the simulated galaxies that form in their highest resolution simulations have many of the properties of observed massive ellipticals — in particular, no ongoing gas accretion and star formation. Maybe smooth accretion comes to a natural end, with no need for AGN feedback or other suppression mechanisms.

However, the story does not appear to be quite so simple. In our simulations, the fraction of cooling halos increases towards lower masses, and while we find some density cores even in halos of  $\sim 10^{12}M_{\odot}$ , core formation is not enough to shut down gas cooling in most halos in the  $10^{12}M_{\odot} - 10^{13}M_{\odot}$  range. If we remove hot mode accretion and cold drizzle in massive halos “by hand,” then we find that the most mas-

sive galaxies are predominantly “red and dead,” in agreement with the high resolution results of Naab et al. (2007). However, in Paper II we show that the simulated massive galaxies are too massive by a factor of 2 – 5 compared to observed galaxies of the same space density, so in the absence of feedback the processes simulated here and by Naab et al. (2007) do not appear able to reproduce the galaxy baryonic mass function; at a given halo mass, galaxies in the real universe are less massive. On the other hand, we also show in Paper II that reproducing observed specific star formation rates requires that central galaxies in a sizeable fraction of  $10^{12} - 10^{13} M_{\odot}$  halos remain on the star forming sequence, so a complete shutdown of accretion above  $10^{12} M_{\odot}$  is not what is desired. Finally, we note again that ejective, galactic wind feedback in lower mass galaxies will ultimately have significant impact on the most massive galaxies by reducing the stellar and gas masses of galaxies that merge with them, by increasing the overall IGM gas supply, and by enriching the IGM and therefore enhancing cooling rates. Our findings here are important steps towards understanding the physics of galaxy growth, and they differ in some significant ways from conventional wisdom, but they do not provide a full solution to the puzzles of observed galaxy evolution.

## 5 CONCLUSIONS

Our principal results are based on a cosmological SPH simulation of a  $50h^{-1}$  Mpc (comoving) box in a  $\Lambda$ CDM universe, evolved with  $288^3$  dark matter and  $288^3$  gas particles using the code GADGET-2. The combination of volume and particle number allows us to resolve (with  $> 64$  particles) galaxies of baryonic mass  $M_{\text{gal}} \gtrsim 6 \times 10^9 M_{\odot}$  while following the formation of several cluster-size halos with  $M_{\text{halo}} \gtrsim 10^{14} M_{\odot}$ . Relative to the main simulation analyzed by K05, our present simulation has an eleven times larger volume, and it uses the entropy-conserving SPH formulation of Springel & Hernquist (2002), which should provide a more accurate treatment of multi-phase gas than the PTreeSPH code employed by K05. We incorporate photoionization by the UV background and thermal feedback on a 2-phase galaxy interstellar medium, but we do not explicitly add galactic winds or track metal enrichment, so this is a “minimal feedback” simulation.

Confirming the key result of K05, we find that galaxies with baryonic masses below  $2 - 3 \times 10^{10} M_{\odot}$  or halo masses below  $2 - 3 \times 10^{11} M_{\odot}$  gain most of their mass through “cold” accretion of gas that has never been close to the halo virial temperature (see also Kay et al. 2000; Fardal et al. 2001; Katz et al. 2003). In halos below  $\sim 2.5 \times 10^{11} M_{\odot}$ , the majority of intergalactic gas is colder than 250,000 K, while in higher mass halos the majority of gas is close to the virial temperature; the transition mass stays nearly constant from  $z = 3$  to  $z = 0$ . Similar behavior is found in spherically symmetric calculations (Birnboim & Dekel 2003; Dekel & Birnboim 2006), and the likely cause of the transition is that the short cooling times in low mass halos prevent the formation of a stable virial shock (Birnboim & Dekel 2003; see also Binney 1977; White & Frenk 1991). However, as shown by K05 and illustrated more comprehensively here, halos near and above the transition mass have hot gas halos penetrated by cold gas filaments, which may con-

tinue to feed the central galaxy. Similar results are found in adaptive mesh refinement simulations (Ocvirk et al. 2008; Dekel et al. 2009; see also Dekel & Birnboim (2006) figure 6). At high redshift these cold filaments penetrate close to the halo center, while in high mass halos at  $z < 1$  they are usually truncated or disrupted before reaching the center. The difference likely reflects the higher physical densities and shorter associated cooling times of the high redshift filaments that prevent the expansion of a stable shock (Birnboim & Dekel 2003) in these high density regions.

The key difference between our present results and those of K05 is that *hot* accretion rates are much lower, a consequence of changing to the more accurate, entropy-conserving SPH formulation. Because of the low hot accretion rates, the growth of high redshift galaxies ( $z \geq 2$ ) is dominated by cold accretion at all galaxy and halo masses. At lower redshifts, massive halos experience a combination of hot accretion and “cold drizzle,” accreting lumps of cold gas below our 64-particle galaxy resolution threshold. Our resolution tests here and those of Naab et al. (2007) suggest that some or even most of this “cold drizzle” may be a numerical artifact. Eliminating it would significantly affect the predicted star formation rates and colors of massive galaxies, but it would not have much impact on their predicted stellar masses (Paper II). At *all* galaxy masses, the majority of galaxy baryonic mass in our simulation was originally acquired by cold accretion, either directly onto the main progenitor or onto a satellite that merged with it.

Galaxy accretion rates decline systematically from  $z = 4$  to  $z = 2$  to  $z = 1$  to  $z = 0$ . For  $10^{10} M_{\odot} < M_{\text{gal}} < 10^{11} M_{\odot}$ , there is a trend of increasing accretion rate with increasing mass at all redshifts, though it becomes flatter at low  $z$ . At higher masses, accretion rates have large scatter and are sensitive to cold drizzle. With our adopted star formation prescription, empirically motivated by the Kennicutt-Schmidt law (Kennicutt 1998; Schmidt 1959), star formation closely tracks gas accretion with a short delay; K05 showed this on a global basis, and here we show it on a galaxy-by-galaxy basis. At each redshift, more massive galaxies tend to have higher star formation rates but (moderately) lower specific star formation rates. Satellite galaxies orbiting within the virial radius of larger halos experience continuing accretion and star formation. The differences in the accretion rates of central and satellite galaxies of the same mass are small at high redshift, while at low redshift a significant fraction of satellites have much lower accretion rates. More detailed analysis of the satellite accretion and merger rates (based on the K05 simulation) appears in Simha et al. (2008).

The low hot accretion rates in our simulated massive halos arise because these halos typically have cores in their hot gas density profiles (or, more precisely, because they break from an approximately  $r^{-2}$  profile to a much shallower profile in their inner regions). By  $z = 0$ , a modest fraction of the  $M > 10^{14} M_{\odot}$  halos develop cuspy density profiles with cooling cores, evolution that is reminiscent of Vikhlinin et al.’s (2007) finding that cooling flow clusters are fairly common at  $z = 0$  but much rarer at  $z > 0.5$ . We speculate that the cores are produced by shocks during the chaotic, rapid assembly phase of halos, and that the more quiescent evolution during the slow accretion phase allows cooling to establish a cusped profile. The accretion rates of central galaxies in our massive halos are predicted

with reasonable accuracy by instantaneous cooling calculations that use the actual simulated gas density profiles, but cooling calculations that assume isothermal gas in equilibrium in an NFW halo or singular isothermal halo may overestimate the cooling rates by orders of magnitude. Our simulation predicts low hot accretion rates even though it does not include AGN heating or other forms of preventive feedback. While such feedback may be needed to explain the absence of cold gas in cooling flow clusters (Kaastra et al. 2001; Peterson et al. 2003), semi-analytic models may overestimate its global importance by assuming incorrect halo gas profiles (and thus excessive cooling).

The comparison to observations in Paper II shows that this simulation, despite its low hot accretion rates, overpredicts the galaxy baryonic mass function. The amount of baryons that is locked in galaxies at  $z = 0$  and the amount of baryons locked in stars at  $z = 0$  is about a factor of 2-3 higher than observed. This is caused by simulated galaxies being too massive at all masses, but the exact difference is a function of galaxy mass with the lowest and the highest mass galaxies being the most problematic. Matching observations therefore requires either the suppression of cold accretion (which seems unlikely on physical grounds) or substantial amounts of ejective feedback that returns gas to the IGM before it forms stars. Such ejective feedback is also needed to explain the observed enrichment of the IGM (e.g., Oppenheimer & Davé 2006, 2008). Ejected, metal-enriched gas will affect the cooling of the IGM in massive halos, and it will reduce the rate at which mergers add stars and gas to massive galaxies. We will investigate the impact of winds and metal-enrichment on galaxy growth in future work with simulations that include these effects. However, our present results suggest that the cooling of shock-heated, virialized gas, which has been the focus of many analytic models of galaxy growth spanning more than three decades, might be a relatively minor element of galaxy formation.

We thank V. Springel for making the GADGET-2 public and K. Finlator and B. Oppenheimer for help during the modification of the public version of the code. D.K. acknowledges the support from the ITC Fellowship at the Institute for Theory and Computation at the Harvard College Observatory. We also acknowledge support from NSF grant AST-0205969 and from NASA grants NAGS-13308 and NNG04GK68G.

## REFERENCES

- Agertz O., Moore B., Stadel J., Potter D., Miniati F., Read J., Mayer L., Gawryszczak A., Kravtsov A., Nordlund Å., Pearce F., Quilis V., Rudd D., Springel V., Stone J., Tasker E., Teyssier R., Wadsley J., Walder R., 2007, MNRAS, 380, 963
- Baldry I. K., Glazebrook K., Brinkmann J., Ivezić Ž., Lupton R. H., Nichol R. C., Szalay A. S., 2004, ApJ, 600, 681
- Barnes J., Hut P., 1986, Nature, 324, 446
- Bell E. F., de Jong R. S., 2000, MNRAS, 312, 497
- Bell E. F., McIntosh D. H., Katz N., Weinberg M. D., 2003, ApJS, 149, 289
- Benson A. J., Pearce F. R., Frenk C. S., Baugh C. M., Jenkins A., 2001, MNRAS, 320, 261
- Bertschinger E., 1989, ApJ, 340, 666
- Best P. N., Kauffmann G., Heckman T. M., Brinchmann J., Charlot S., Ivezić Ž., White S. D. M., 2005, MNRAS, 362, 25
- Binney J., 1977, ApJ, 215, 483
- Binney J., 2004, MNRAS, 347, 1093
- Birnboim Y., Dekel A., 2003, MNRAS, 345, 349
- Bower R. G., Benson A. J., Malbon R., Helly J. C., Frenk C. S., Baugh C. M., Cole S., Lacey C. G., 2006, MNRAS, 370, 645
- Bullock J. S., Kolatt T. S., Sigad Y., Somerville R. S., Kravtsov A. V., Klypin A. A., Primack J. R., Dekel A., 2001, MNRAS, 321, 559
- Burns J. O., Hallman E. J., Gantner B., Motl P. M., Norman M. L., 2008, ApJ, 675, 1125
- Cattaneo A., Blaizot J., Weinberg D. H., Kereš D., Colombi S., Davé R., Devriendt J., Guiderdoni B., Katz N., 2007, MNRAS, 377, 63
- Cattaneo A., Dekel A., Devriendt J., Guiderdoni B., Blaizot J., 2006, MNRAS, 370, 1651
- Cattaneo A., Dekel A., Faber S. M., Guiderdoni B., 2008, MNRAS, 389, 567
- Cole S., Aragon-Salamanca A., Frenk C. S., Navarro J. F., Zepf S. E., 1994, MNRAS, 271, 781
- Conroy C., Ostriker J. P., 2008, ApJ, 681, 151
- Croft R. A. C., Di Matteo T., Davé R., Hernquist L., Katz N., Fardal M. A., Weinberg D. H., 2001, ApJ, 557, 67
- Croton D. J., Springel V., White S. D. M., De Lucia G., Frenk C. S., Gao L., Jenkins A., Kauffmann G., Navarro J. F., Yoshida N., 2006, MNRAS, 365, 11
- Daddi E., Dickinson M., Morrison G., Chary R., Cimatti A., Elbaz D., Frayer D., Renzini A., Pope A., Alexander D. M., Bauer F. E., Giavalisco M., Huynh M., Kurk J., Mignoli M., 2007, ApJ, 670, 156
- Davé R., 2008, MNRAS, 385, 147
- De Grandi S., Molendi S., 2002, ApJ, 567, 163
- Dekel A., Birnboim Y., 2006, MNRAS, 368, 2
- Dekel A., Birnboim Y., 2008, MNRAS, 383, 119
- Dekel A., Birnboim Y., Engel G., Freundlich J., Goerdt T., Mumcuoglu M., Neistein E., Pichon C., Teyssier R., Zinger E., 2009, Nature, 457, 451
- Dekel A., Silk J., 1986, ApJ, 303, 39
- Di Matteo T., Springel V., Hernquist L., 2005, Nature, 433, 604
- Efstathiou G., 1992, MNRAS, 256, 43P
- Erb D. K., Steidel C. C., Shapley A. E., Pettini M., Reddy N. A., Adelberger K. L., 2006, ApJ, 646, 107
- Fabian A. C., 1994, ARA&A, 32, 277
- Fardal M. A., Katz N., Gardner J. P., Hernquist L., Weinberg D. H., Davé R., 2001, ApJ, 562, 605
- Gingold R. A., Monaghan J. J., 1977, MNRAS, 181, 375
- Gunn J. E., Gott J. R. I., 1972, ApJ, 176, 1
- Haardt F., Madau P., 2001, in Neumann D. M., Tran J. T. V., eds, Clusters of Galaxies and the High Redshift Universe Observed in X-rays Modelling the UV/X-ray cosmic background with CUBA
- Hatton S., Devriendt J. E. G., Ninin S., Bouchet F. R., Guiderdoni B., Vibert D., 2003, MNRAS, 343, 75
- Hernquist L., 1987, ApJS, 64, 715
- Hockney R. W., Eastwood J. W., 1981, Computer Simulation Using Particles. Computer Simulation Using Particles, New York: McGraw-Hill, 1981

- Hopkins A. M., Beacom J. F., 2006, *ApJ*, 651, 142
- Hopkins P. F., Cox T. J., Kereš D., Hernquist L., 2008, *ApJS*, 175, 390
- Kaastra J. S., Ferrigno C., Tamura T., Paerels F. B. S., Peterson J. R., Mittaz J. P. D., 2001, *A&A*, 365, L99
- Katz N., 1992, *ApJ*, 391, 502
- Katz N., Keres D., Dave R., Weinberg D. H., 2003, in Rosenberg J. L., Putman M. E., eds, *ASSL Vol. 281: The IGM/Galaxy Connection. The Distribution of Baryons at  $z=0$  How Do Galaxies Get Their Gas?*. pp 185–+
- Katz N., Weinberg D. H., Hernquist L., 1996, *ApJS*, 105, 19
- Kauffmann G., Heckman T. M., White S. D. M., Charlot S., Tremonti C., Peng E. W., Seibert M., Brinkmann J., Nichol R. C., SubbaRao M., York D., 2003, *MNRAS*, 341, 54
- Kauffmann G., White S. D. M., Guiderdoni B., 1993, *MNRAS*, 264, 201
- Kay S. T., Pearce F. R., Jenkins A., Frenk C. S., White S. D. M., Thomas P. A., Couchman H. M. P., 2000, *MNRAS*, 316, 374
- Kennicutt Jr. R. C., 1998, *ApJ*, 498, 541
- Keres D., 2007, PhD thesis, University of Massachusetts Amherst
- Keres D., Katz N., Dave R., Fardal M., Weinberg D. H., 2009, *ArXiv e-prints:0901.1880*
- Kereš D., Katz N., Weinberg D. H., Davé R., 2005, *MNRAS*, 363, 2
- Khochfar S., Ostriker J. P., 2008, *ApJ*, 680, 54
- Li Y., Mo H. J., van den Bosch F. C., Lin W. P., 2007, *MNRAS*, 379, 689
- Lucy L. B., 1977, *AJ*, 82, 1013
- Maller A. H., Bullock J. S., 2004, *MNRAS*, 355, 694
- Maller A. H., Katz N., Kereš D., Davé R., Weinberg D. H., 2006, *ApJ*, 647, 763
- McKee C. F., Ostriker J. P., 1977, *ApJ*, 218, 148
- McNamara B. R., Nulsen P. E. J., 2007, *ARA&A*, 45, 117
- Mo H. J., Miralda-Escude J., 1996, *ApJ*, 469, 589
- Mo H. J., Yang X., van den Bosch F. C., Katz N., 2005, *MNRAS*, 363, 1155
- Morandi A., Ettori S., 2007, *MNRAS*, 380, 1521
- Murali C., Katz N., Hernquist L., Weinberg D. H., Davé R., 2002, *ApJ*, 571, 1
- Naab T., Johansson P. H., Ostriker J. P., Efstathiou G., 2007, *ApJ*, 658, 710
- Navarro J. F., Frenk C. S., White S. D. M., 1997, *ApJ*, 490, 493
- Noeske K. G., et al., 2007, *ApJL*, 660, L43
- Ocvirk P., Pichon C., Teyssier R., 2008, *MNRAS*, 390, 1326
- Oppenheimer B. D., Davé R., 2006, *MNRAS*, 373, 1265
- Oppenheimer B. D., Davé R., 2008, *MNRAS*, 387, 577
- Pearce F. R., Jenkins A., Frenk C. S., White S. D. M., Thomas P. A., Couchman H. M. P., Peacock J. A., Efstathiou G., 2001, *MNRAS*, 326, 649
- Peterson J. R., Kahn S. M., Paerels F. B. S., Kaastra J. S., Tamura T., Bleeker J. A. M., Ferrigno C., Jernigan J. G., 2003, *ApJ*, 590, 207
- Quinn T., Katz N., Efstathiou G., 1996, *MNRAS*, 278, L49
- Rees M. J., Ostriker J. P., 1977, *MNRAS*, 179, 541
- Schmidt M., 1959, *ApJ*, 129, 243
- Silk J., 1977, *ApJ*, 211, 638
- Simha V., Weinberg D. H., Dave R., Gnedin O. Y., Katz N., Keres D., 2008, *ArXiv e-prints:0809.2999*
- Somerville R. S., Primack J. R., 1999, *MNRAS*, 310, 1087
- Spergel D. N., et al., 2007, *ApJS*, 170, 377
- Springel V., 2005, *MNRAS*, 364, 1105
- Springel V., Hernquist L., 2002, *MNRAS*, 333, 649
- Springel V., Hernquist L., 2003, *MNRAS*, 339, 289
- Thoul A. A., Weinberg D. H., 1996, *ApJ*, 465, 608
- Tinker J. L., Weinberg D. H., Zheng Z., Zehavi I., 2005, *ApJ*, 631, 41
- Tittley E. R., Pearce F. R., Couchman H. M. P., 2001, *ApJ*, 561, 69
- van den Bosch F. C., Mo H. J., Yang X., 2003, *MNRAS*, 345, 923
- Vikhlinin A., Burenin R., Forman W. R., Jones C., Hornstrup A., Murray S. S., Quintana H., 2007, in Böhringer H., Pratt G. W., Finoguenov A., Schuecker P., eds, *Heating versus Cooling in Galaxies and Clusters of Galaxies Lack of Cooling Flow Clusters at  $z \lesssim 0.5$* . pp 48–+
- Wadsley J. W., Stadel J., Quinn T., 2004, *New Astronomy*, 9, 137
- Weinmann S. M., van den Bosch F. C., Yang X., Mo H. J., Croton D. J., Moore B., 2006, *MNRAS*, 372, 1161
- White S. D. M., Frenk C. S., 1991, *ApJ*, 379, 52
- White S. D. M., Rees M. J., 1978, *MNRAS*, 183, 341